NASA TechBriefs

National Aeronautics and
Space Administration

Electronic Components and Circuits

Electronic Systems

Physical Sciences

Materials

Computer Programs

Mechanics

Machinery

Fabrication Technology

Mathematics and Information Sciences

Life Sciences

INTRODUCTION

Tech Briefs are short announcements of innovations originating from research and development activities of the National Aeronautics and Space Administration. They emphasize information considered likely to be transferable across industrial, regional, or disciplinary lines and are issued to encourage commercial application.

Availability of NASA Tech Briefs and TSPs

Requests for individual Tech Briefs or for Technical Support Packages (TSPs) announced herein should be addressed to

National Technology Transfer Center
Telephone No. **(800) 678-6882** or via World Wide Web at **www2.nttc.edu/leads/**

Please reference the control numbers appearing at the end of each Tech Brief. Information on NASA's Commercial Technology Team, its documents, and services is also available at the same facility or on the World Wide Web at **www.nctn.hq.nasa.gov**.

Commercial Technology Offices and Patent Counsels are located at NASA field centers to provide technology-transfer access to industrial users. Inquiries can be made by contacting NASA field centers and program offices listed below.

NASA Field Centers and Program Offices

Ames Research Center
Carolina Blake
(650) 604-0893 or
cblake@mail.arc.nasa.gov

Dryden Flight Research Center
Lee Duke
(805) 258-3802 or
lee.duke@dfrc.nasa.gov

Goddard Space Flight Center
George Alcorn
(301) 286-5810 or
galcorn@gsfc.nasa.gov

Jet Propulsion Laboratory
Merle McKenzie
(818) 354-2577 or
merle.mckenzie@ccmail.jpl.nasa.gov

Johnson Space Center
Hank Davis
(281) 483-0474 or
hdavis@gp101.jsc.nasa.gov

John F. Kennedy Space Center
Gale Allen
(407) 867-6626 or
galeallen-1@ksc.nasa.gov

Langley Research Center
Dr. Joseph S. Heyman
(804) 864-6006 or
j.s.heyman@larc.nasa.gov

Glenn Research Center
Larry Viterna
(216) 433-3484 or
cto@lerc.nasa.gov

George C. Marshall Space Flight Center
Sally Little
(256) 544-4266 or
sally.little@msfc.nasa.gov

John C. Stennis Space Center
Kirk Sharp
(228) 688-1929 or
ksharp@ssc.nasa.gov

NASA Program Offices
At NASA Headquarters there are seven major program offices that develop and oversee technology projects of potential interest to industry:

Carl Ray
Small Business Innovation Research Program (SBIR) & Small Business Technology Transfer Program (STTR)
(202) 358-4652 or
cray@mail.hq.nasa.gov

Dr. Robert Norwood
Office of Aeronautics and Space Transportation Technology (Code R)
(202) 358-2320 or
rnorwood@mail.hq.nasa.gov

John Mulcahy
Office of Space Flight (Code MP)
(202) 358-1401 or
jmulcahy@mail.hq.nasa.gov

Gerald Johnson
Office of Aeronautics (Code R)
(202) 358-4711 or
g_johnson@aeromail.hq.nasa.gov

Bill Smith
Office of Space Science (Code S)
(202) 358-2473 or
wsmith@sm.ms.ossa.hq.nasa.gov

Roger Crouch
Office of Microgravity Science Applications (Code U)
(202) 358-0689 or
rcrouch@hq.nasa.gov

Granville Paules
Office of Mission to Planet Earth (Code Y)
(202) 358-0706 or
gpaules@mtpe.hq.nasa.gov

BLANK PAGE

NASA TechBriefs

National Aeronautics and Space Administration

August 1999
19-08

BLANK PAGE

Electronic Components and Circuits

Hardware, Techniques, and Processes

BLANK PAGE

Three-Phase Sine-Wave Generator

A circuit generates three-phase sine waves with excellent amplitude and phase symmetry.

John H. Glenn Research Center, Cleveland, Ohio

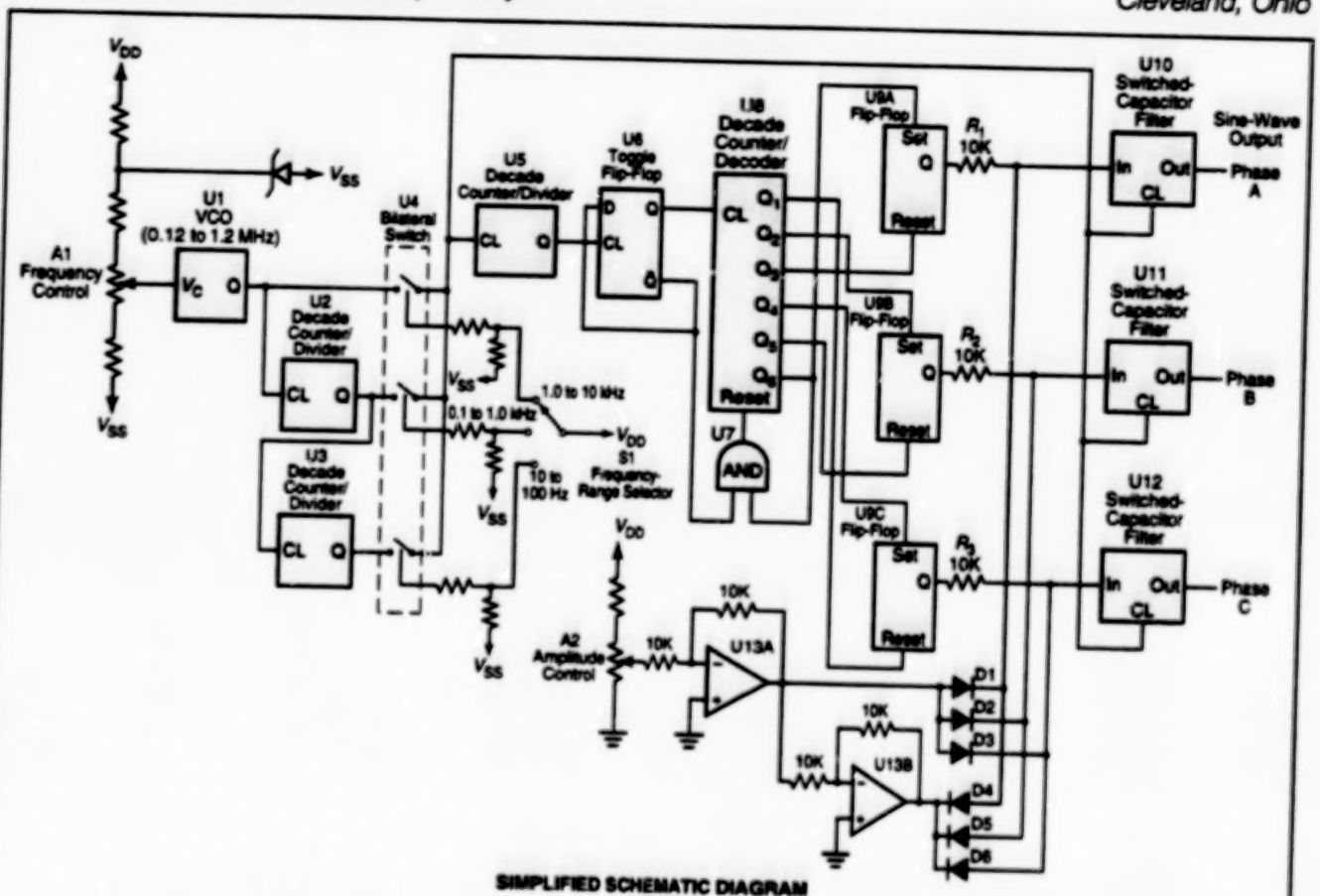

SIMPLIFIED SCHEMATIC DIAGRAM

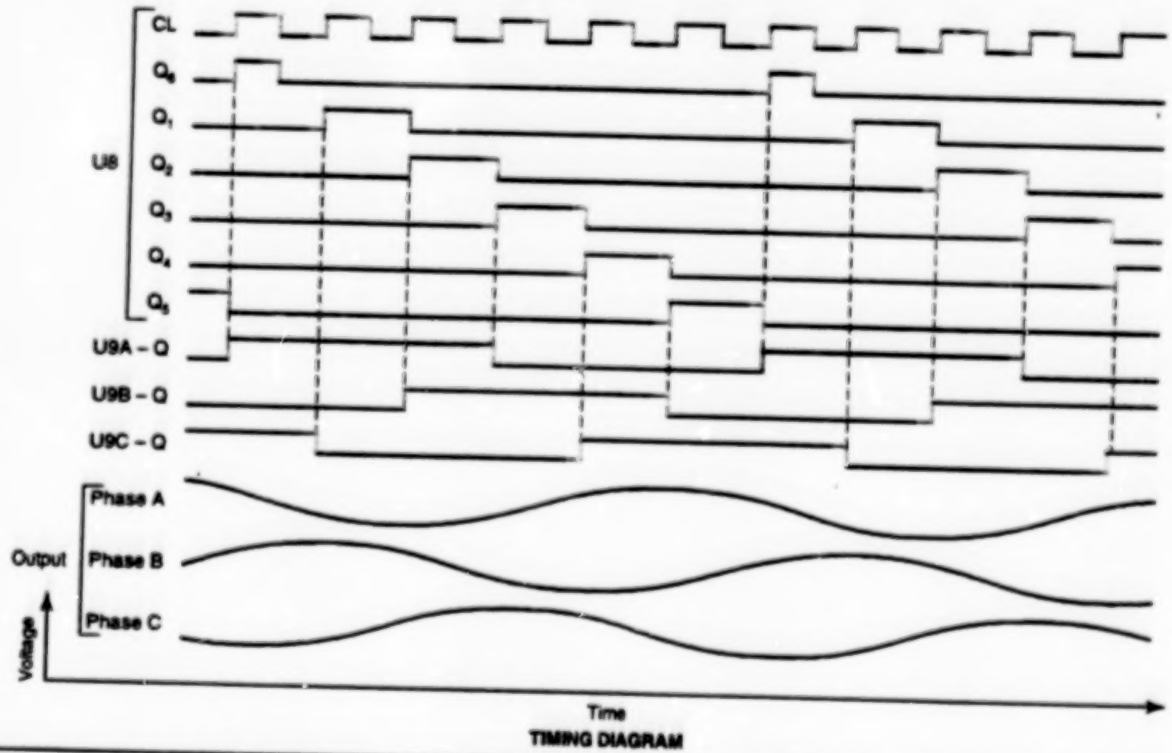

TIMING DIAGRAM

This **Three-Phase Sine-Wave Generator** is an inexpensive digital/analog circuit assembled from complementary metal oxide/semiconductor (CMOS) integrated circuits and other components.

A variable-frequency, three-phase, sine-wave generator circuit has been designed for use as a source of polyphase excitation in studies of the propagation of traveling waves in plasmas. This circuit, combined with three power-amplifier channels and three high-voltage transformers, is used to power the plasma apparatus that is used in the studies.

The circuit (see figure) internally generates three symmetrical square-wave voltages with precisely 120° phase difference, each square wave containing only odd harmonics. Three switched-capacitor, six-pole Butterworth low-pass filters (U10, U11, and U12) remove the harmonics but pass the fundamental sine-wave component.

The operating-frequency range of the circuit, 10 Hz to 10 kHz, is covered in three decade ranges. A Zener-stabilized voltage-controlled oscillator (VCO) functions as a variable-frequency oscillator and covers just over one decade, while a switch-selectable frequency-divider chain (U2, U3, and U4) provides frequency-range selection by decades.

The operating frequency is 1/120th of the switched-capacitor filter clocking frequency. This frequency-division ratio is set by a fixed frequency-divider chain (U5, U6, U7, and U8). Inasmuch as this ratio is constant, the low-pass-filter cutoff frequency automatically tracks the operating frequency.

Decade counter/decoder U8 generates set and reset pulses in the proper sequence for flip-flops U9A, U9B, and U9C. In turn, these flip-flops generate symmetrical square-wave voltages. Once each cycle, AND gate U7 resets counter/decoder U8 to count zero after U8 reaches a count of six.

The amplitude of the sine-wave voltages generated by this circuit is proportional to the amplitude of the square wave at the filter input. The square-wave voltages are symmetrically clamped by diodes D1 through D6. The peak-to-peak voltage swing is limited by the total dc voltage developed at the outputs of operational amplifiers U13A and U13B. Amplitude control A2 sets the bias on the operational amplifiers, thereby setting the square-wave amplitude and ultimately the sine-wave amplitude. Controlling the amplitude in this way ensures that the amplitudes of the three sine waves track each other accurately over a wide range of amplitude settings.

Because dc control of amplitude and frequency is used in this design, the frequency- and amplitude-control components (A1, S1, and A2) can be located remotely without affecting the quality of the three-phase sine-wave signals.

This work was done by R. Ziemke of **Glenn Research Center.** *Further information is contained in a TSP [see page 1].*

Inquiries concerning rights for the commercial use of this invention should be addressed to NASA Glenn Research Center, Commercial Technology Office, Attn: Steve Fedor, Mail Stop 4–8, 21000 Brookpark Road, Cleveland, Ohio 44135. Refer to LEW-16696.

Microwave Heating of Fibers for Chemical Vapor Deposition

Multiple fibers, either electrically conductive or nonconductive, can be coated simultaneously.

NASA's Jet Propulsion Laboratory, Pasadena, California

A microwave-cavity applicator has been developed for coating multiple fibers by chemical vapor deposition (CVD). A prototype of the applicator was used to deposit silicon carbide onto carbon fibers; the design of the applicator can just as well be optimized for coating fibers made of other materials, and for depositing coating materials other than SiC.

There are two conventional techniques for CVD on fibers. In one technique, a fiber is pulled through a chamber that contains CVD reagent gases. The fiber enters and leaves the chamber through mercury electrodes that also serve as gas seals. The fiber is heated to the reaction temperature by an electrical current applied through the mercury electrode/seals. The disadvantages of this technique are that it is limited to electrically conductive fibers, each reaction chamber can accommodate only one fiber at a time, and the toxicity of mercury poses a hazard. In the other conventional technique, a fiber is heated in a waveguide-type microwave applicator. Although this technique is not limited to electrically conductive fibers and does not involve mercury, it, too, is limited to one fiber per applicator, and the waveguide applicator is intrinsically energy-inefficient because its proper operation depends upon absorption of a substantial portion of the incident microwave power in a dummy load.

The present microwave-cavity applicator overcomes the disadvantages of the applicators used in both conventional techniques: It can be used to coat multiple fibers, the fibers can be electrically conductive or nonconductive, there is no need for mercury, and microwave energy is utilized more efficiently than in the older waveguide/dummy-load microwave applicator.

The enhancement in energy efficiency is achieved by use of a resonant microwave cavity and by positioning the fibers in the cavity so as to cause only a small deviation of the electromagnetic field from the empty-cavity normal mode while causing the fibers to absorb a large fraction of the microwave power that enters the cavity. The positioning is especially critical for coating fibers of carbon and other lossy materials; typically, such fibers should be placed near an electric-field node.

The figure is a simplified drawing of the applicator. The major structural component is a circular cylindrical microwave cavity. Microwave power is supplied through a coaxial transmission line and coupled into the cavity by a coaxial rod antenna.

The electromagnetic field in the chamber is excited in a close approximation of a TM_{0N0} mode, where N is a positive integer. (The mode would be purely TM_{0N0}, were it not for the small perturbations introduced by the objects described below.) The TM_{0N0} mode is axisymmetric; therefore, to expose multiple fibers to identical microwave conditions, one need only take care to position the fibers and other objects symmetrically about the axis of the cavity.

The cavity contains multiple (four in the example of the figure) reaction

chambers in the form of tubes made of quartz or other low-loss dielectric material. The reaction chambers are placed at equal angular intervals and nominally at the same radius. In operation, reagent gases are made to flow through the reaction chambers while the fibers are pulled through the reaction chambers and heated to the CVD reaction temperature by the microwave field.

Efficient utilization of the incident microwave power depends critically on good impedance matches from the transmission line through the antenna to the partially filled cavity, then to the fibers. The length of the rod antenna can be adjusted for an impedance match from the transmission line to the chamber. The fibers must be positioned at an optimum radius, which is nearer or farther from an electric-field node, depending on whether the fibers are more or less lossy. Slots in the end plates of the cavity accommodate adjustments in the radial positions of the reaction chambers and thus of the fibers.

This work was done by Henry W. Jackson of Acro Service Corp. and Martin Barmatz and Gordon Hoover of Caltech for **NASA's Jet Propulsion Laboratory**. *Further information is contained in a TSP [see page 1].*

In accordance with Public Law 96-517, the contractor has elected to retain title to this invention. Inquiries concerning rights for its commercial use should be addressed to

Technology Reporting Office
JPL
Mail Stop 122-116
4800 Oak Grove Drive
Pasadena, CA 91109
(818) 354-2240

Refer to NPO-20458, volume and number of this NASA Tech Briefs *issue, and the page number.*

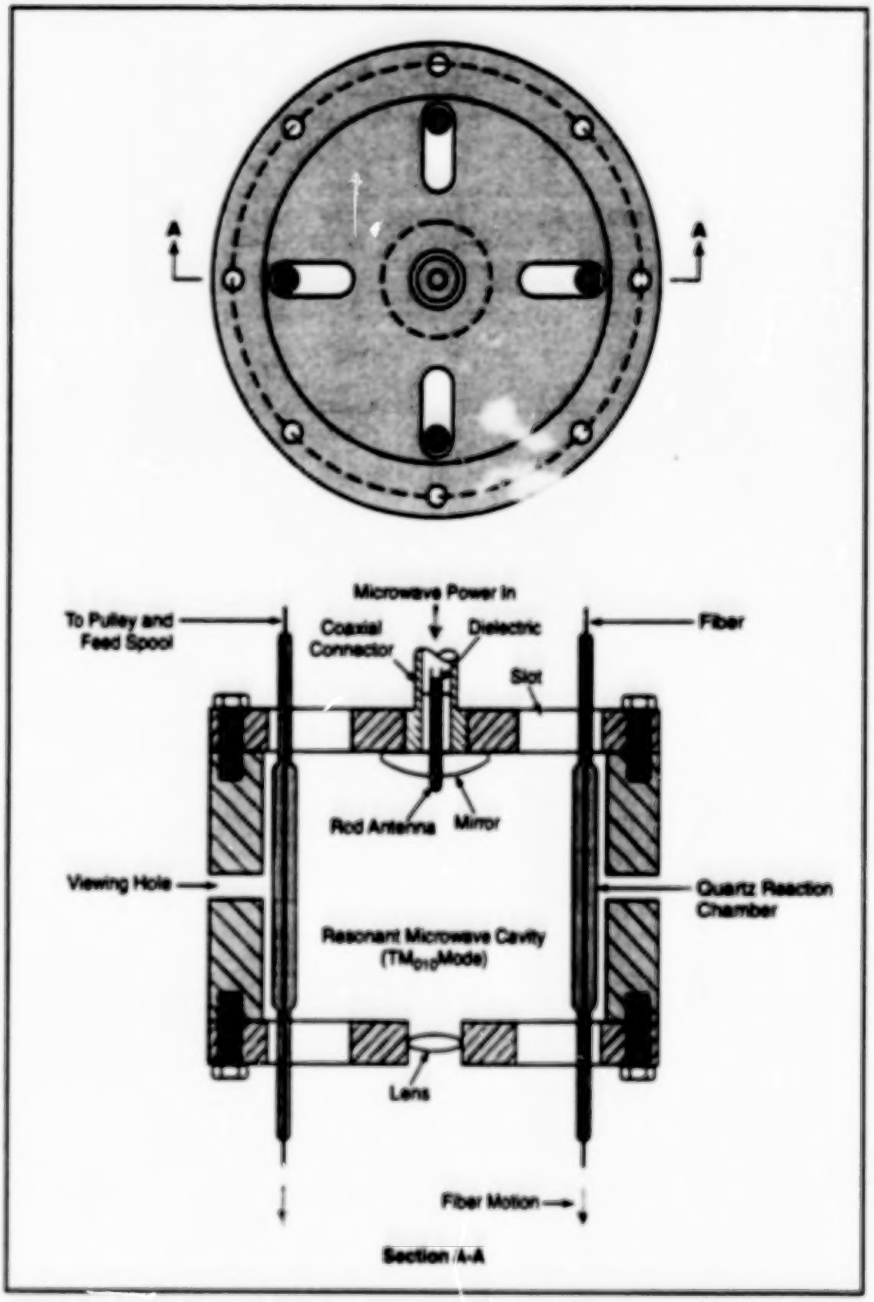

Fibers Are Pulled Through Reaction Chambers filled with CVD reagent gases in a resonant microwave cavity. The microwave field heats the fibers to the CVD reaction temperature. Although four reaction chambers are shown here, more or fewer could be included. The curved mirror and lens can be used for optical monitoring of the process.

BLANK PAGE

Physical Sciences

Hardware, Techniques, and Processes

12

BLANK PAGE

Exploiting Crossed Magnetic Antennas in a Natural Waveguide

An electrical discharge could be located through observation from a single site.

Goddard Space Flight Center, Greenbelt, Maryland

A technique that involves the use of crossed magnetic antennas in a natural waveguide has been proposed for tracking Martian dust storms from a single observing station; that is, without having to triangulate from multiple observing stations. The technique is applicable to tracking thunderstorms on Earth.

An electromagnetic wave propagating in a waveguide exhibits dispersion; that is, the components of the wave at different frequencies propagate at different speeds and arrive at a receiving site at different times. Because the degree of dispersion is cumulative with distance, a measurement of dispersion can be used to estimate the distance a wave has traveled.

A highly electrically conductive ionosphere and the ground below it constitute a natural waveguide. Within this waveguide, powerful low-frequency electromagnetic signals, like those generated by intense electrical discharges (e.g., lightning strokes) can travel great distances. Provided that a sufficiently sensitive radio spectrometer is used to measure the dispersion of a wave, the distance from a receiver to a lightning stroke or other source of the wave can be estimated fairly precisely from the measured dispersion, even if the distance is thousands of kilometers. Furthermore, by using two crossed magnetic antennas (search coils) to measure mutually perpendicular horizontal components of the magnetic field of the wave, one obtains the information needed to calculate the azimuth of the source. Thus, the location of source, projected onto the ground surface, can be fully determined.

Electrical discharges are expected to occur on Mars. These discharges are expected to arise from dust storms, instead of from thunderstorms as on Earth and elsewhere in the Solar system. Electrically charged dust storms may act to transfer electrical currents across long filamentary paths and may thereby radiate at frequencies <10 kHz. By exploiting the propagation of such waves within the natural waveguide between the Martian ionosphere and ground surface, one would determine the locations of the discharges according to the principle described above and would thus be able to track the dust storms from one site on the surface. The range of detectability for the instrument is determined, in part, by the ground conductivity (i.e., conductivity of lower boundary of the waveguide) with reduced attenuation associated with lower conductivities. Thus, an estimate of Martian subsurface conductivity can also be derived by the variation of discharge signal strength with distance.

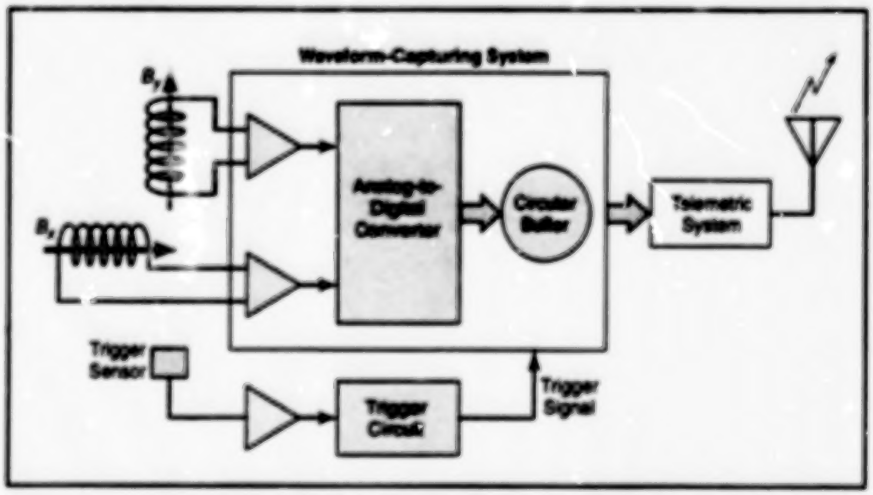

This Instrument Would Sample the B_x and B_y Waveforms. The sample data would be processed to determine the range and azimuth of an electrical discharge.

An incoming electromagnetic wave would have magnetic vector components B_x and B_y where x and y denote mutually perpendicular coordinate axes aligned approximately with corresponding mutually perpendicular axes of sensitivity of two search coils. Measurements of the waveforms and analyses of the spectra of both B_x and B_y would be needed to determine the degree of dispersion and the azimuth. The results of the dispersion and azimuth calculations would be used, in turn, to estimate the distance and direction to the source of the wave. Waveform analysis would require sampling of B_x and B_y at a rate of approximately 20 kS/s.

The figure is a system-level block diagram of an instrument that would perform the necessary measurements and would not impose excessive demands on telemetric resources. The instrument would include two search coils mounted with their axes of sensitivity orthogonal to each other in a horizontal plane. The outputs of the coils would be fed to a waveform-capturing system (WCS).

WCS would accumulate data continually in a circular buffer which would pass the data to a telemetry buffer on command. The command would be issued in response to a trigger signal generated by an external sensor whenever the sensor detected a discharge event. (The external sensor could be a photometer, vertical electric-field sensor, or other device that is particularly sensitive to broadband signals from lightninglike discharges.) Thus, the only data returned by the instrument would be those obtained around the time of a discharge, and the telemetric data rate averaged over long observing time would thereby be kept low. Each set of data thus returned would be used to compute the distance and direction to a source.

This work was done by W. Farrell, M. Desch, M. Kaiser, and J. Houser of **Goddard Space Flight Center.** *No further documentation is available.*

GSC-13976

BLANK PAGE

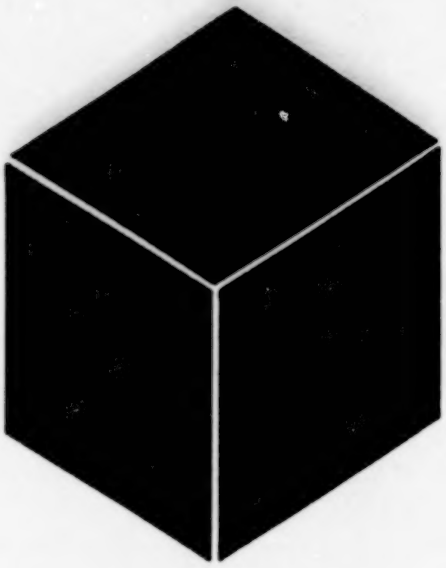

Materials

Hardware, Techniques, and Processes

16

BLANK PAGE

Polycrystalline Tb/Dy Alloy for Magnetostrictive Actuators

The cheaper polycrystalline version gives about 60 percent of the single-crystal magnetostriction.

NASA's Jet Propulsion Laboratory, Pasadena, California

Research has shown that with suitable processing, one can produce a polycrystalline version of a terbium/dysprosium alloy suitable for use in a magnetostrictive actuator for generating small motions. Prior to this research, only the single-crystal version had been used, and that in only a limited number of applications. One advantage of polycrystalline Tb/Dy is that it costs much less than does the single-crystal version. A second advantage of the polycrystalline material is that the preload springs, which are necessary in most single-crystal applications, can be eliminated in many cases.

Magnetostrictive actuators are attractive for generating motion at cryogenic temperatures, where piezoelectric actuators lose much of their effectiveness. The Tb/Dy alloy exhibits a large magnetostriction at low temperatures, with the ratio of Tb to Dy chosen so that the anisotropy is minimized for the temperature range of operation.

The raw polycrystalline material is produced by casting. To obtain sufficient actuation performance (see figure) that results in saturation magnetostriction, which is 60 percent of the saturation magnetostriction of single-crystal Tb/Dy, it is necessary to orient a substantial fraction of the crystal grains by a suitable mechanical treatment. Experiments have shown that by rolling the cast material and subjecting the rolled material to multiple heat treatments, one can achieve a degree of crystalline orientation that results in 60 percent of the magnetostriction of single-crystal Tb/Dy; even at this reduced level, the low-temperature actuation performance of polycrystalline Tb/Dy is still about 50 times that of a piezoelectric material.

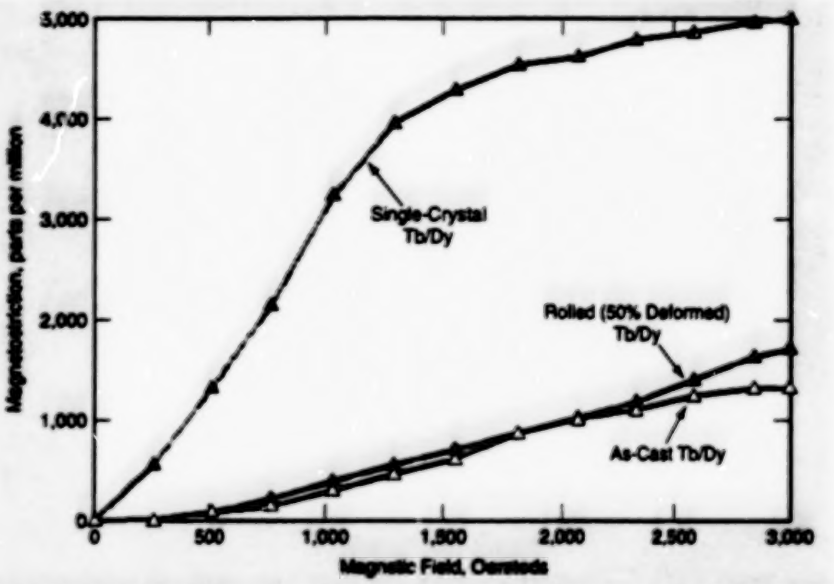

Magnetostriction Was Measured in specimens of Tb/Dy at a temperature of 77 K. Rolled Tb/Dy performed somewhat better than did as-cast Tb/Dy. Experiments have shown that optimized thermomechanical treatment can produce an even bigger increase in magnetostriction, up to a major fraction of the magnetostriction of single-crystal Tb/Dy.

This work was done by Robert Chave, Christian Lindensmith, Jennifer Dooley, Brent Fultz, and Marius Birsan of Caltech for **NASA's Jet Propulsion Laboratory**. *Further information is contained in a TSP [see page 1].*

In accordance with Public Law 96-517, the contractor has elected to retain title to this invention. Inquiries concerning rights for its commercial use should be addressed to

Technology Reporting Office
JPL
Mail Stop 122-116
4800 Oak Grove Drive
Pasadena, CA 91109
(818) 354-2240

Refer to NPO-20273, volume and number of this NASA Tech Briefs *issue, and the page number.*

Extruding Tb/Dy for Magnetostrictive Actuators

Extrusion would yield the required crystal orientation and would be suited to mass production.

NASA's Jet Propulsion Laboratory, Pasadena, California

A process that is undergoing development would be used to mass-produce textured polycrystalline rods of a terbium/dysprosium alloy for cryogenic magnetostrictive actuators. The rolling-and-heat-treatment process described in the preceding article yields a high degree of crystal orientation, but is suitable for small batches only. The developmental process is expected to be inexpensive to provide greater uniformity in larger batches in a mass-production setting.

The process exploits an established coextrusion technique in which a tube is filled with a material, then the tube and its contents are redrawn to a smaller diameter. The uniform stretch of the tube and its contents yields a high degree of orientation of crystals along the axis of the tube.

First, the unoriented polycrystalline Tb/Dy is encased in a tube of 316L stainless steel. Then the filled tube is drawn through a die sized to increase the length of the tube by a factor of 4. Finally, the tube is split to remove the polycrystalline Tb/Dy rod. The degree of parallel alignment and long-axis orientation of the crystals in the drawn rod is sufficient for an effective magnetostrictive actuator.

This work was done by Robert Chave, Jennifer Dooley, Brent Fultz, and Marius Birsan of Caltech for **NASA's Jet Propulsion Laboratory**. *Further information is contained in a TSP [see page 1].*

In accordance with Public Law 96-517, the contractor has elected to retain title to this invention. Inquiries concerning rights for its commercial use should be addressed to

Technology Reporting Office
JPL
Mail Stop 122-116
4800 Oak Grove Drive
Pasadena, CA 91109
(818) 354-2240

Refer to NPO-20277, volume and number of this NASA Tech Briefs *issue, and the page number.*

Magnetostrictive Micropositioner for Cryogenic Applications

This nonbackdriveable mechanism generates small increments of motion with long overall travel.

NASA's Jet Propulsion Laboratory, Pasadena, California

A Magnetostrictive Inertial-Reaction-Motor Rotary Drive is combined with a threadless rotary-to-linear clutch to obtain axial motion of the shaft, with very small steps, self-braking, and capability of operation in a cryogenic system.

A magnetostrictive linear-translation mechanism has been designed to function as a micropositioning device at any temperature from ambient down to the temperature of liquid helium (about 4 K). Still undergoing development at the time of reporting the information for this article, this magnetostrictive micropositioner is a prototype of micropositioners for a variety of room-temperature and low-temperature applications in which there are requirements for high stiffness, increments of motion < 1 μm, and long travel (through concatenated multiple small increments). Such micropositioners could be used to make fine position adjustments in diverse scientific and industrial instruments; for example, they could be used to drive translation stages in scanning tunneling microscopes or to move optical elements that must be located at long but precise distances from each other (as in telescopes and interferometers).

Magnetostrictive micropositioners that act in "inchworm" fashion were reported in "Magnetostrictive Actuators for Cryogenic Applications" (NPO-19218), *NASA Tech Briefs*, Vol. 20, No. 3 (March 1996), page 84. Magnetostrictive micropositioners that exploit a combination of stick/slip and inertial effects were reported in "Magnetostrictive Inertial-Reaction Linear Motors" (NPO-20153), *NASA Tech Briefs*, Vol. 22, No. 6 (June 1998), page 66. The present magnetostrictive micropositioner shares some characteristics with the inchworm and inertial-reaction types; like an inchworm actuator, it is nonbackdriveable and self-braking (it retains its position when power is not applied), and like an inertial-reaction actuator, it exploits a combination of stick/slip and inertial effects. However, the present magnetostrictive micropositioner features a distinct design that addresses major issues of lubrication and energy efficiency that arise in a cryogenic environment.

The prime mover in this micropositioner is a linear actuator that comprises (a) a single crystal of the magnetostrictive rare-earth alloy $Tb_{0.74}Dy_{0.26}$ surrounded by (b) high-temperature-superconductor solenoid. The superconductivity of the solenoid minimizes electric power dissipation, thereby contributing to energy efficiency and to reduction of waste heat (which must be removed to maintain a cryogenic environment).

The reason for choosing a magnetostrictive (instead of, say, a piezoelectric) actuator to obtain small increments of motion is that magnetostrictive actuators function throughout the desired temperature range and even work better as temperature decreases, whereas piezoelectric actuators tend to become inoperable in cryogenic environments. $Tb_{0.74}Dy_{0.26}$ was chosen because it exhibits a large magnetostrictive effect in the intended operating-temperature range; for example, application of a magnetic flux density of 1,000 G to a 20-mm-long $Tb_{0.74}Dy_{0.26}$ crystal produces a stroke as large as 0.1 mm. The use of a single crystal of magnetostrictive material contributes further to energy efficiency and reduction of waste heat, in that relative to polycrystalline mass, a single crystal undergoes much less heating when magnetostrictively flexed.

The magnetostrictive crystal is connected to a linear-to-rotary clutch. The solenoid is driven with a sawtooth signal, causing the crystal to repeatedly extend slowly and snap back rapidly. The motion of the crystal drives a pendulum that is lightly spring-loaded against a drive shaft. The slow extension of the crystal causes the shaft to rotate through a small increment of angle in one direction. However, the force of the snap-back acceleration is greater than the force of friction between the pendulum and the drive shaft, so that the shaft does not rotate in the opposite direction. The cycle then repeats, producing another increment of shaft rotation. Of course, the shaft can be made to rotate in repeated increments in the opposite direction by reversing the polarity of the drive waveform.

By use of a little known but highly reliable rotary-to-linear clutch, the rotary motion of the drive shaft is used to obtain lengthwise motion of the shaft. The rotary-to-linear clutch includes six small bearings that are spring-loaded against the drive shaft in two groups of three bearings each. The axes of the bearings are skewed slightly from the axis of the shaft, so that each incremental rotation of the shaft causes the shaft to advance lengthwise by an amount that depends on the skew angle and the diameter of the shaft (2 μm of advance per degree of rotation in the present design). The rotary-to-linear clutch provides the desired self-braking and nonbackdriveability, and the spring loading affords compliance needed to tolerate changes in temperature.

At the time of reporting the information for this article, there were no lubricants suitable for long-term cryogenic sliding mechanical contacts like those of lead screws in conventional linear actuators. The use of rolling-contact bearings in the present magnetostrictive micropositioner obviates the issue of lubrication of sliding contacts. The rolling contacts are lubricated with molybdenum disulfide, which is a proven low-temperature solid lubricant for ball bearings.

In a test at room temperature, this magnetostrictive micropositioner was found to be capable of producing linear position increments of about 1 μm. With further refinement, it should be possible to achieve increments as small as 0.1 μm. The overall travel is limited only by the length of the drive shaft; a typical overall travel of 10 cm is easily achieved.

This work was done by Robert Chave of Caltech for ***NASA's Jet Propulsion Laboratory****. Further information is contained in a TSP [see page 1].*

In accordance with Public Law 96-517, the contractor has elected to retain title to this invention. Inquiries concerning rights for its commercial use should be addressed to

Technology Reporting Office
JPL
Mail Stop 122-116
4800 Oak Grove Drive
Pasadena, CA 91109
(818) 354-2240

Refer to NPO-20270, volume and number of this NASA Tech Briefs *issue, and the page number.*

Magnetostrictive Filter-Wheel Drive

This drive could be operated at any temperature from ambient down to near absolute zero.

NASA's Jet Propulsion Laboratory, Pasadena, California

The figure shows a prototype of a magnetostrictively actuated mechanism that would rotate an optical filter wheel for a high-performance infrared camera or telescope. Typically, a high-performance infrared instrument and its filter wheel are operated inside a cryogenic system. In conventional practice, the filter wheel is turned by use of a stepping motor in a warmer location. The mechanical connection between the stepping motor and the filter wheel is designed to be as thermally isolating as possible, but it still leaks appreciable heat into the cryogenic system. In contrast, the magnetostrictive drive can be operated with minimal heat leakage because it can be mounted inside the cryogenic system along with the filter wheel and infrared instrument. Moreover, in comparison with a stepping-motor drive, the magnetostrictive drive is simpler, less expensive, and more reliable.

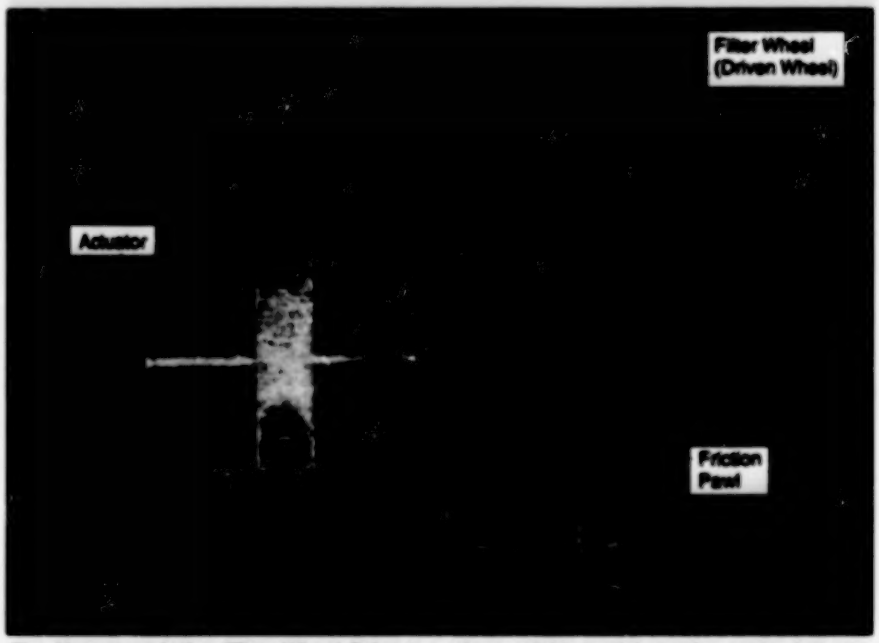

The Magnetostrictive Filter-Wheel Drive is a robust, reliable inertial-reaction motor that contains only a few moving parts. When operated in a cryogenic system, it contributes minimally to the heat load.

The magnetostrictive drive is an inertial-reaction motor; that is, a motor that exploits a combination of stick/slip and inertial effects. A linear actuator in frictional contact with an armature (in this case, the wheel) is excited by a sawtooth signal, causing one end of the actuator to repeatedly accelerate slowly in one direction, then rapidly in the reverse direction back to the starting point. Because of the frictional contact, the armature moves with the end of the actuator during the initial slow acceleration. However, the force of the reverse acceleration is greater than the frictional force between the actuator and the armature, so that the armature does not snap back along with the actuator. The cycle then repeats, producing another increment of armature motion (in this case, an increment of rotation of the wheel). By reversing the polarity of the sawtooth waveform, one can reverse the direction of motion.

In this case, the linear actuator is a magnetostrictive rod connected to a friction pawl that makes contact with the wheel. When no power is applied to the actuator, friction holds the wheel in position. The magnetostrictive material is a terbium/dysprosium alloy, which exhibits a large magnetostriction at cryogenic temperatures. To minimize the heat load of the cryogenic system, the magnetostrictive rod can be driven by use of a superconducting solenoid. For an operating temperature of about 77 K (liquid-nitrogen temperature), one would have to use a solenoid made of a high-temperature superconductor.

In a test at a temperature of 77 K, the magnetostrictive drive was found to produce rotation with angular increments as small as an arc second and with a slew rate as high as 1.5 r/min. Inasmuch as the magnetostrictive rod generates a longer stroke at lower temperature, it should be possible to achieve a greater slew rate at the typical liquid-helium temperature of 4 K.

This work was done by Robert Chave and Christian Lindensmith of Caltech for ***NASA's Jet Propulsion Laboratory****. Further information is contained in a TSP [see page 1].*

In accordance with Public Law 96-517, the contractor has elected to retain title to this invention. Inquiries concerning rights for its commercial use should be addressed to

Technology Reporting Office
JPL
Mail Stop 122-116
4800 Oak Grove Drive
Pasadena, CA 91109
(818) 354-2240

Refer to NPO-20275, volume and number of this NASA Tech Briefs *issue, and the page number.*

Push/Pull Magnetostrictive Linear Actuator

"Inchworm" motion would be achieved by a combination of magnetostriction and magnetic clamping.

NASA's Jet Propulsion Laboratory, Pasadena, California

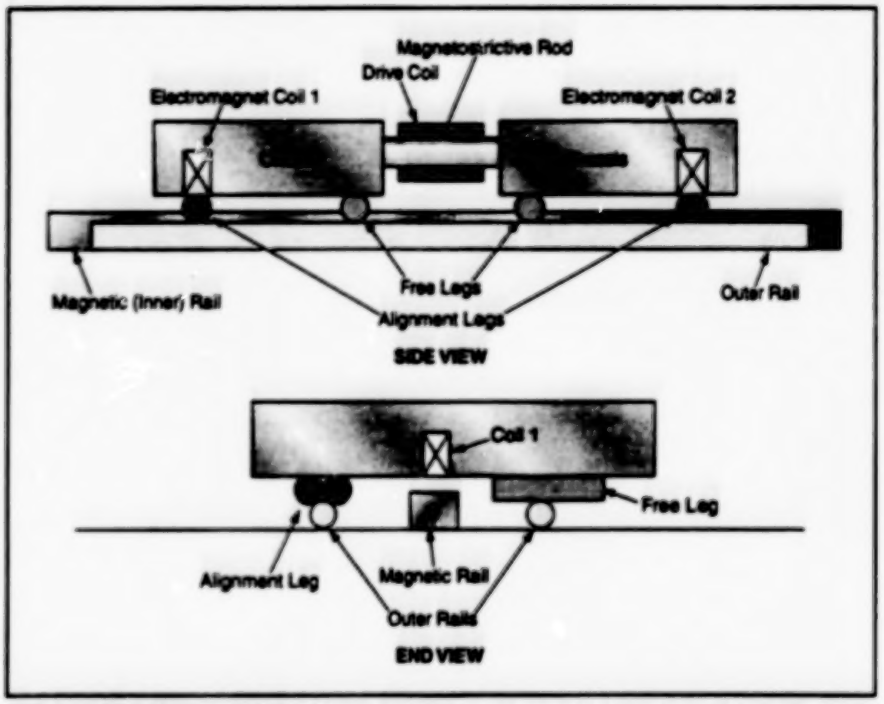

The Push/Pull Magnetostrictive Linear Actuator would move in a sequence of magnetic clamping and unclamping of the two chassis coordinated with energizing and deenergizing the drive coil on the magnetostrictive rod.

A proposed "kinematic inchworm"-type linear actuator would move a mass as large as 2 kg along rails, with lengthwise position controllable in increments as small as 50 nm. The actuator could be operated in microgravity or in normal Earth gravitation and at any temperature from ambient down to cryogenic. The actuator could be used, for example, to position an optical assembly precisely on a long interferometer arm, as a translation stage for a scanning tunneling microscope, or as a translation stage for inspecting integrated-circuit chips.

The figure schematically illustrates the proposed actuator as it would be used to move a stage along two parallel outer rails. The stage would include two chassis connected lengthwise by a magnetostrictive device, which would comprise a Tb/Dy-alloy rod surrounded by a drive coil. The kinematic relationship between the outer rails and the stage would be established by free legs and alignment legs on the two chassis. A noncontact inner rail made of a magnetic material would lie between the two outer rails. Each chassis would contain an electromagnet coil above the magnetic rail; this coil could be energized to provide a clamping force and an associated frictional force that would prevent the chassis from sliding along the outer rails.

Referring to the figure, a cycle of operation to move the stage one increment of distance to the right would comprise the following steps:

1. Coil 1 would be energized to clamp the left chassis in place.
2. The drive coil would be energized, causing the magnetostrictive rod to lengthen slightly, thereby pushing the right chassis a short distance to the right. The power would have to be applied to the drive coil gradually enough not to generate sufficient inertial force to overcome the friction holding the left chassis in place.
3. Coil 2 would be energized to clamp the right chassis in place.
4. Coil 1 would be deenergized, leaving the left chassis free to slide along the rails.
5. The drive coil would be deenergized, causing the magnetostrictive rod to shorten slightly, thereby pulling the left chassis to the right. At this point, both chassis would have moved one increment to the right.

The cycle could be repeated as many times as needed to move the stage a required distance to the right. By simply interchanging coils 1 and 2 in the sequence, one could obtain motion from right to left.

The size of the increment could be controlled by varying the current applied to the drive coil. Position feedback could be used for precise control of motion. For operation in a cryogenic system, it would be best if the drive and electromagnet coils were made of superconductive material to minimize waste heat. It would be especially desirable to use superconductive coils with persistent-current switches if electromagnetic clamping were to be used to hold the stage once it reached the desired final position.

This work was done by Robert Chave, Christian Lindensmith, Jennifer Dooley, Brent Fultz, and Marius Birsan of Caltech for **NASA's Jet Propulsion Laboratory**. *Further information is contained in a TSP [see page 1].*

In accordance with Public Law 96-517, the contractor has elected to retain title to this invention. Inquiries concerning rights for its commercial use should be addressed to

Technology Reporting Office
JPL
Mail Stop 122-116
4800 Oak Grove Drive
Pasadena, CA 91109
(818) 354-2240

Refer to NPO-20272, volume and number of this NASA Tech Briefs *issue, and the page number.*

Improved Magnetostrictive Valve for Use at Low Temperature

Careful design provides for low heat leakage and low dead volume.

NASA's Jet Propulsion Laboratory, Pasadena, California

An improved magnetostrictive valve for remotely controlling a flow of liquid helium has been developed. Heretofore, flows of liquid helium have been controlled by use of valves with mechanical or gas connections to actuators in warmer locations. The connections act as heat-leak paths. In contrast, the design of the present valve is optimized for operation at liquid-helium

temperature (below 4.2 K), so that the entire valve can be maintained at or slightly above liquid-helium temperature to minimize leakage of heat into the liquid helium.

A valve with some similarities to the present one was described in "Magnetostrictive Valve for Use at Low Temperature" (NPO-19480), *NASA Tech Briefs*, Vol. 21, No. 2 (February 1997), page 14b.The poppet in this valve, as in the previous one, is a ball contained in a passage between an inlet and an outlet. In this case, the ball is made of 440C and is of high sphericity [root-mean-square deviation < 5 μin. (0.127 μm)]. The valve seat is made of superclean, fine-grained 316L steel and is initially lapped to optical flatness. In a later stage of fabrication, the ball is used to "coin" the seat.

As in the previous valve, the actuator in this valve is a magnetostrictive device comprising a rod of terbium/dysprosium alloy surrounded by a solenoidal drive coil that generates the magnetic field needed for actuation. The Tb/Dy alloy was chosen because it exhibits a large magnetostriction in the intended cryogenic operational temperature range. The Tb/Dy rod is mounted in such a way as to provide for removal and installation of different drive coils. To minimize generation of heat in the cryogenic environment, a superconductive drive coil can be used. For temperatures up to 77 K, one can use high-temperature superconductor; for liquid-helium temperature, one can use a superconductive Nb/Ti alloy.

Stainless filters containing submicron pores are inserted in the inlet and outlet ports of the valve to prevent particulate contamination and thereby prolong the operational life of the valve. The "dead" volume in this valve is only 6 μL on the outlet side. In tests at a temperature of 77 K, the valve withstood 300 actuations, with no sign of helium leakage. The valve was also tested at 4.2 K for several actuations with no sign of helium leakage.

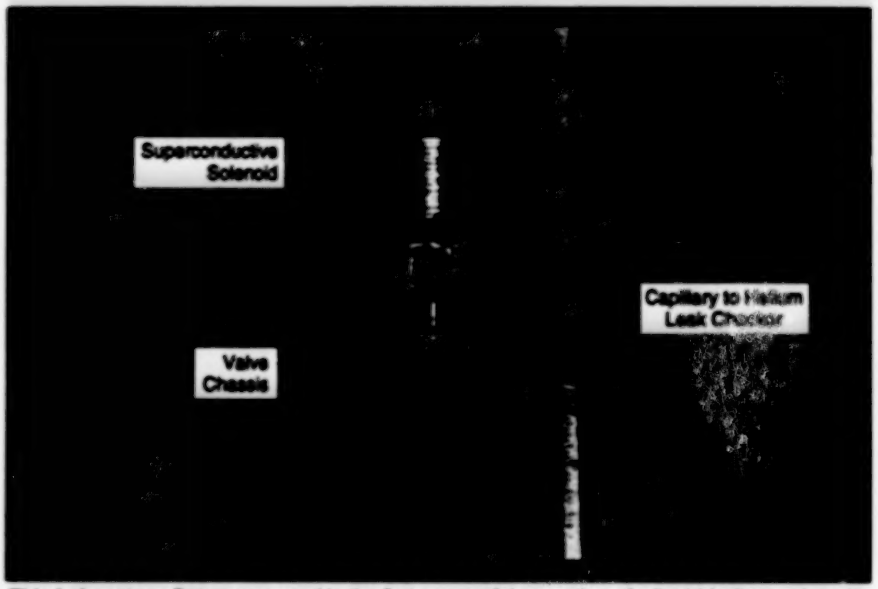

This Laboratory Setup was used in the first successful operation of a liquid-helium valve with a magnetostrictive actuator driven by a high-temperature-superconductor solenoid.

This work was done by Robert Chave, Christian Lindensmith, Jennifer Dooley, Brent Fultz, and Marius Birsan of Caltech for **NASA's Jet Propulsion Laboratory**. *Further information is contained in a TSP [see page 1].*

In accordance with Public Law 96-517, the contractor has elected to retain title to this invention. Inquiries concerning rights for its commercial use should be addressed to

Technology Reporting Office
JPL
Mail Stop 122-116
4800 Oak Grove Drive
Pasadena, CA 91109
(818) 354-2240

Refer to NPO-20271, volume and number of this NASA Tech Briefs *issue, and the page number.*

Magnetostrictive Heat Switch for Cryogenic Use

This switch would be superior to both gas-gap and externally mechanically actuated switches.

NASA's Jet Propulsion Laboratory, Pasadena, California

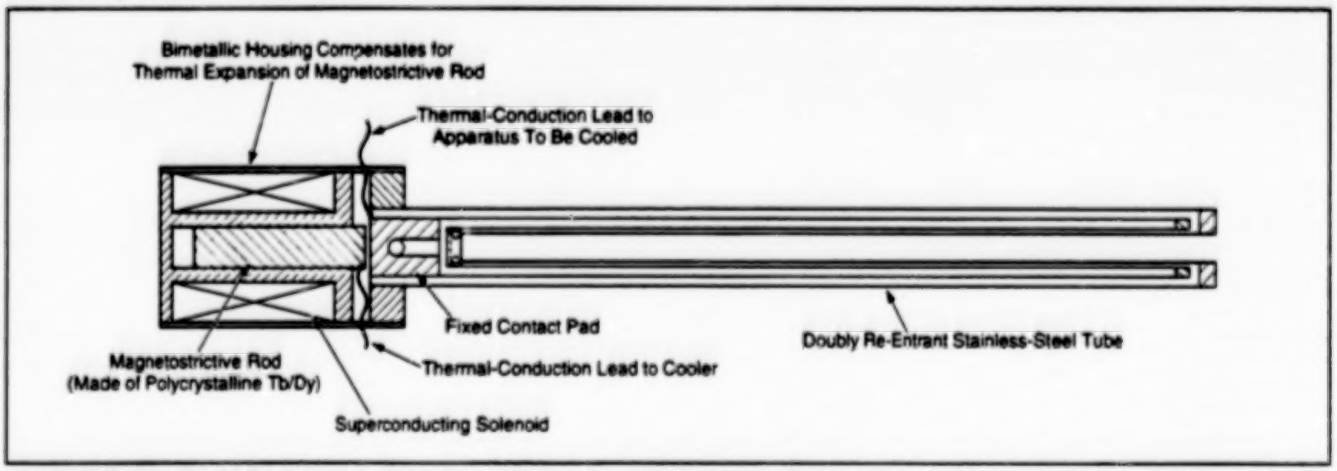

The **Heat Switch Would Be Closed or Opened** by exploiting the magnetostrictive effect to make or break a mechanical contact along the main heat-conduction path.

A magnetostrictively actuated heat switch has been proposed for use in a variety of cryogenic equipment, including adiabatic-demagnetization refrigerators, calorimeters, and coolers for high-performance infrared cameras. Heretofore, the heat switches in such equipment have generally been of two types: gas-gap and externally mechanically actuated. The gas-

gap switches are limited to long cycle times and tend to exhibit both poor isolation in their "open" states and low "closed"/"open" heat-transfer ratios. In the case of externally mechanically actuated switches, the mechanical connections between the switches and the outside environment are heat-conduction paths, along which heat leaks into the affected cryogenic chambers. In contrast, the proposed magnetostrictively actuated switch would feature short cycle times, low heat leakage, high isolation in the "open" state, and a high "closed"/"open" ratio.

As shown in the figure, the main thermal contact in the switch would be made or broken by making or breaking, respectively, the mechanical contact between (1) the moving end of a rod of magnetostrictive material and (2) a fixed contact pad. The magnetostrictive material would be a terbium/dysprosium alloy, which exhibits a large magnetostrictive effect at low temperature. The use of a polycrystalline form of this alloy would eliminate the need for a return spring that must be used with the single-crystal form of the alloy, enabling a reduction in the weight and complexity of the switch. The magnetic field needed for actuation would be generated by use of a superconducting solenoid made of Nb/Ti alloy.

In operation, the superconducting solenoid would generate no waste heat. The entire switch, including the magnetostrictive actuator and superconducting solenoid, would be mounted at the cold stage used for temperature control. By using superconducting leads to the cold stage, the heat leak to the cold stage would be minimized. The switch would be mounted on a stainless-steel tube with a doubly reentrant design that provides good thermal isolation in a small space; the estimated open-state thermal conductance of the assembly is 15 μW/K.

This work was done by Robert Chave, Christian Lindensmith, Brent Fultz, and Marius Birsan of Caltech for **NASA's Jet Propulsion Laboratory**. *Further information is contained in a TSP [see page 1].*

In accordance with Public Law 96-517, the contractor has elected to retain title to this invention. Inquiries concerning rights for its commercial use should be addressed to

Technology Reporting Office
JPL
Mail Stop 122-116
4800 Oak Grove Drive
Pasadena, CA 91109
(818) 354-2240

Refer to NPO-20274, volume and number of this NASA Tech Briefs *issue, and the page number.*

Computer Programs

BLANK PAGE

Mechanics

Program Estimates Loads in Launch Vehicles

This program saves time in preliminary design and analysis.

Version 1.4 of the Launch Vehicle Loads Analysis for Preliminary Design (VLOADS 1.4) computer program calculates in-flight launch-vehicle structural loads (that is, spacecraft-launching rockets) for preliminary design. The program can also be used to calculate structural loads in upper stages and planetary-transfer spacecraft.

VLOADS compiles and analyzes launch-vehicle information such as aerodynamic coefficients, mass properties, data on propellants, and engine thrusts, to calculate distributed shear loads, bending moments, axial forces, and vehicle line loads as functions of *X* station (position along the longitudinal axis of the vehicle). If the launch vehicle includes boosters or wings, then VLOADS also computes interface loads.

An attractive feature of VLOADS is that its source code is in Visual Basic for Applications and has been integrated into an easy-to-use Microsoft Excel user interface. VLOADS uses the individual worksheets in its Excel workbook as input and output data files, in a manner similar to the way in which traditional FORTRAN and BASIC programs have used text files as input and output files. Because VLOADS has been integrated into an Excel workbook, it is much easier for the user to edit the input data, run the program, and view the results.

The major strength of VLOADS is that it enables rapid analysis of structural loads in launch vehicles during the preliminary-design phase of development. Thus, VLOADS offers an alternative to the time-consuming and expensive chore of developing finite-element models for detailed analysis of loads. In preliminary design, much remains unknown about the details of the configuration to which the launch vehicle will mature.

It becomes necessary to make some simplifying assumptions to initiate the process by which loads can be calculated for preliminary design and analysis of structures. VLOADS implements a two-degree-of-freedom mathematical model for calculating the distribution of axial force, shear force, and bending moment along the length of the vehicle. The model essentially treats the launch vehicle as a rigid beam; vibrations are not considered. The method of sections is employed to determine the shear, moment, and axial load. Rotational acceleration in the pitch plane is assumed equal to zero, so that the sum of pitching moments equals zero.

VLOADS was developed as a Visual Basic macro in a Microsoft Excel 5.0/95 workbook program on a Power Macintosh computer. VLOADS has also been implemented on a '486-class personal computer using version 7.0a of Microsoft Excel for Windows 95, and on a '586-class personal computer running Windows NT 4.0. The standard distribution medium for VLOADS is one 3.5-in. (8.89-cm), 1.44MB, MS-DOS-format diskette. VLOADS was developed in 1996, and VLOADS 1.4 was released to COSMIC in 1997. The program is copyrighted work with all copyright vested in NASA.

This program was written by Paul L. Luz and Jerry B. Graham of **Marshall Space Flight Center**. *For further information, contact Larry Gagliano at (256) 544-7175.*

MFS-27332

Mathematics and Information Sciences

Software for Detecting Anomalies and Responding to Faults

The Automated Test Monitor computer program provides for continuous monitoring of the operations of a complex system (e.g., a spacecraft). This program implements a rigorous analytic (instead of an *ad hoc*) technique that prescribes exactly how to express requirements for the operation of the system, and how to construct and implement a software subsystem that can detect violations of the requirements. Thus, the program provides a theoretical and computational framework that is potentially applicable to monitoring of a variety of systems. Run-time monitor software is constructed (hereafter, "monitor" for short) that can be embedded in the software that controls the operation of the system to be monitored. In the generation of the monitor, correctness properties are expressed as linear temporal logic (LTL) formulas, then a procedure is generated from the formulas. The system-control software is then modified manually to provide the software analog of instrumentation that informs the monitor of events in the system that can cause changes in LTL correctness properties. The monitor responds whenever it detects an event that violates a specified correctness property. The response of the monitor can be used to activate a subsystem to respond to the fault that caused the violation.

This program was written by Francis Schneider of Caltech for **NASA's Jet Propulsion Laboratory**. *Further information is contained in a TSP [see page 1].*

NPO-20585

BLANK PAGE

Mechanics

Hardware, Techniques, and Processes

BLANK PAGE

Experiment on Reducing Drag on an Aerospace Launch Vehicle

Roughening of the forebody reduces base drag but not overall drag.

Dryden Flight Research Center, Edwards, California

Current proposed shapes for single-stage-to-orbit vehicles like the Lockheed-Martin X-33 and VentureStar reusable launch vehicle have extremely large base areas when compared with previous hypersonic-vehicle designs. As a result, base drag — especially in the transonic flight regime — is expected be very large. The unique configuration of the X-33, with its very large base area and relatively low forebody drag, offers the potential for a very high payoff in overall performance if the base drag can be reduced significantly. This article presents results of a base-drag-reduction experiment that was performed in the X-33 Linear Aerospike SR-71 (LASRE) flight program.

The experiment was a flight test of a roughly 20-percent half-span model of an X-33 forebody with a single aerospike rocket engine at the rear. As shown in Figure 1, the test model was mounted on top of an SR-71 airplane. It was intended that the LASRE flight-test data would be used to define the aerospike-engine performance under realistic flight conditions and to determine interactions of the engine plume with the base and engine cowl areas.

In order to measure performance of the linear aerospike engine under a variety of flight conditions, the model was mounted on the SR-71 with a pylon that was instrumented with 8 load cells oriented to measure total forces and moments in six degrees of freedom. The model was also instrumented with surface pressure ports on the forebody, boat tail, base, engine ramps, and lower engine fence. By numerically integrating the surface pressure distributions obtained from measurements at these surface pressure ports, it was possible to calculate the model profile drag.

Baseline drag measurements on the LASRE configuration demonstrated a large transonic-drag rise that is significantly larger than the wind-tunnel value predicted for the X-33. It is likely that the observed transonic-drag difference is an effect of the sting mount used to support the X-33 wind-tunnel model. With increasing mach number in the subsonic flight regime, base drag (referenced to the LASRE base area) was found to be relatively constant at a base-drag coefficient of approximately 0.38 until the divergence-drag-rise mach number of approximately 0.90 is reached.

It was found that after the divergence mach number is reached, compressibility effects dominate and the base-drag coefficient rises rapidly. Above mach 1, the base-drag coefficient decreases steadily with increasing mach number. In the subsonic flight regime, base drag constitutes approximately 125 percent of the overall model drag. (In the subsonic flight regime, there was considerable suction present on the model forebody. The forebody suction induced a negative forebody pressure drag coefficient of approximately –0.075. The forebody suction results in a drag coefficient for the entire body of approximately 0.30. Thus, in the subsonic flight regime, the base drag was nearly 25 percent larger than the total drag of the vehicle.) Approximately 80 percent of the transonic-drag rise can be attributed to effects of compressibility on base drag. Baseline LASRE drag data clearly support the assertion that base drag dominates the overall drag. If one is to reduce the overall drag of the vehicle, then the base area is clearly the place to start.

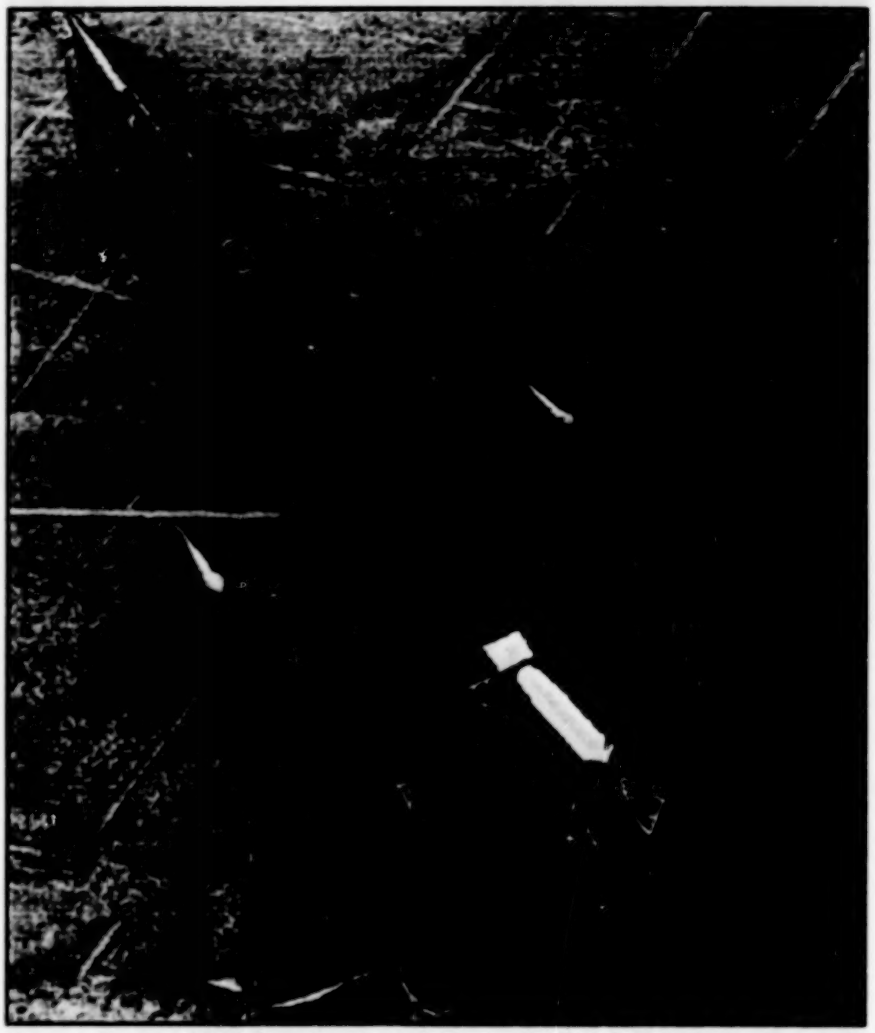

Figure 1. For the LASRE Experiment, a half-span model of an X-33 forebody with a single aerospike rocket engine at the rear was mounted on top of an SR-71 airplane.

In the case of blunt-based objects that feature heavily separated base areas, a clear relationship between base drag and "viscous" forebody drag has been demonstrated. Generally, as the forebody drag on such an object is increased, base drag tends to decrease. This reduction of base drag is a result of boundary-layer effects at the base. The shear layer generated by rubbing of the free-stream flow against the dead, separated air in the base region acts as a jet pump and serves to reduce the pressure coefficient in the base areas. The surface boundary layer acts as an "insulator" between the external flow and the dead air at the base. As the forebody drag is increased, the thickness of boundary layer at the aft end of the forebody increases, with a consequent reduction in the effectiveness of the pumping and a reduction in the base drag. For subsonic flight

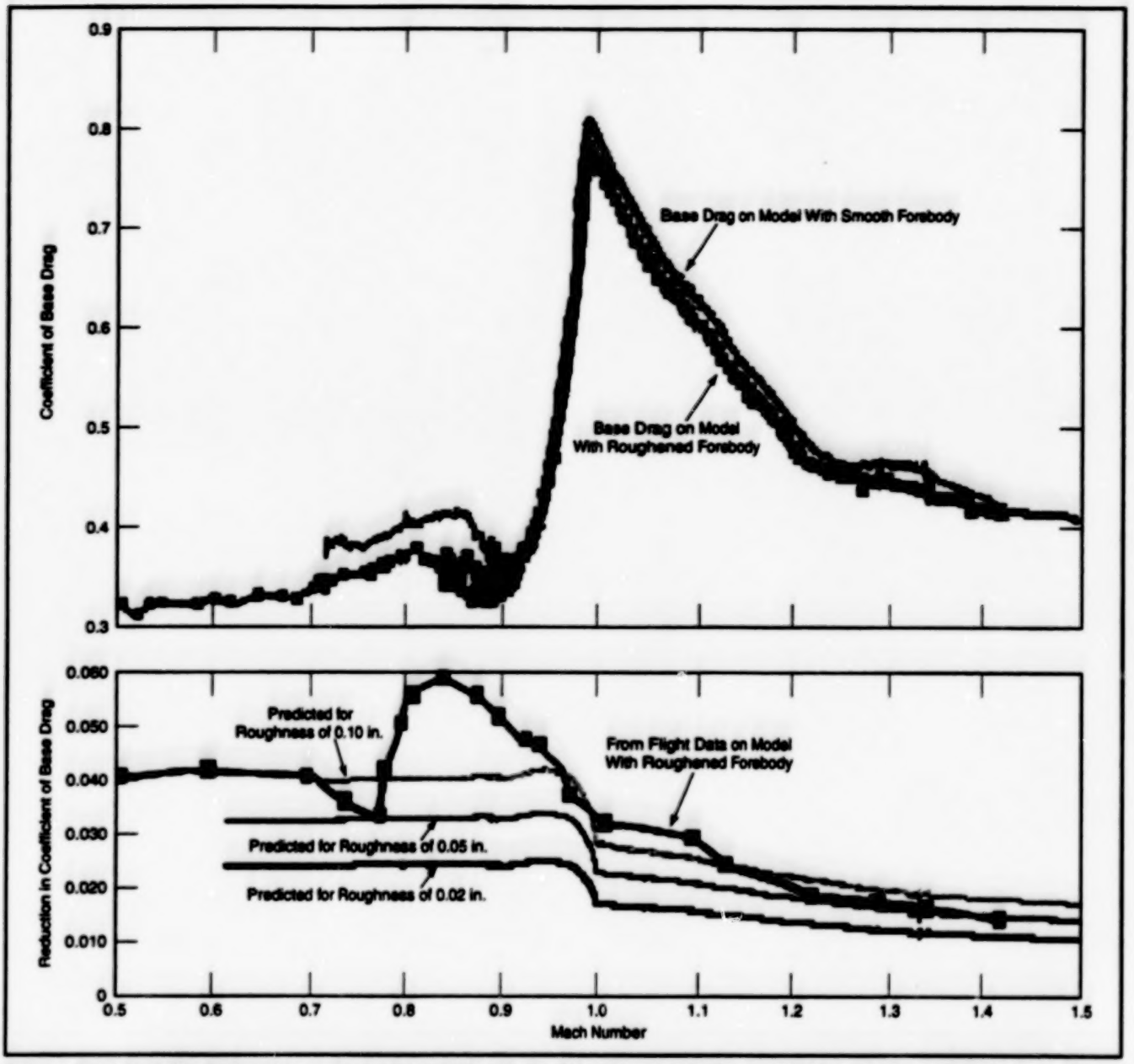

Figure 2. Base Drag Was Reduced by roughening the forebody with grit. The measured reduction exceeded the reduction predicted for three different roughnesses of the order of magnitude of the actual roughness. All of the coefficient values plotted here are referenced to the LASRE base area.

conditions, it has been demonstrated that for objects with base drag coefficients greater than 0.30, the forebody/base drag relationship is extremely sensitive. For these flow conditions, a small increment in the forebody friction drag will result in a relatively large decrease in the base drag of the object. Since the subsonic LASRE base drag coefficient is 0.38, it is expected that the LASRE base drag/forebody drag relationship should exhibit a similar high sensitivity. Conceptually, if the increment in forebody skin drag is optimized with respect to the reduction in base drag, then it may be possible to reduce the overall drag of the configuration.

In the LASRE drag-reduction experiment, researchers sought to increase the forebody skin friction and modify the boundary layer at the back end of the LASRE model. One of the most convenient methods of increasing the forebody skin drag is to add roughness to the surface. Such other methods as the use of vortex generators to energize the boundary layer would probably work more effectively, but the intrusion of vortex generators into the airflow precludes the use of them on hypersonic re-entry vehicles. The benefits of using surface roughness are nonintrusiveness (minimal heating), small weight penalty, mechanical simplicity, and low cost.

For the LASRE drag-reduction experiment, # 24 silicon carbide [0.035 in. (0.9 mm)] grit was glued to the skin by use of spray-on adhesive, and the surface was sealed by use of a high-tensile-strength, heat-resistant, white enamel paint. The resulting surface had an equivalent sand-grain roughness that varied between approximately 0.02 in. (0.5 mm) and 0.05 in. (1.3 mm). In an attempt to avoid inducing additional flow separation at the boat tail or along the forebody, only the flat sides of the LASRE model were gritted. The gritted area covered approximately one-third of the forebody wetted area.

Results of the experiment verified that surface roughness can be effective in reducing base drag. Figure 2 shows the measured reduction in base drag, in comparison with the reductions in base drag predicted for surface roughnesses of 0.02 in. (0.5 mm), 0.05 in. (1.3 mm), and 0.10 in. (2.5 mm). The predicted reductions in base drag ranged from 8 to

14 percent. The base-drag reduction calculated from flight data peaked at 15 percent. The base-drag reduction also persisted well out into the supersonic flight regime. Since base drags of supersonic projectiles had never before been correlated with viscous forebody drags, the sizable reduction in supersonic base drag in this experiment was a significant positive result.

Unfortunately, flight-test results for the rough-surface configuration did not demonstrate an overall net reduction of drag. The surface grit caused a rise in forebody pressures. Coupled with increased forebody skin drag, the forebody pressure rise offset benefits gained by reducing base drag. Clearly the techniques used to apply the surface grit must be refined. In addition, the existence of an optimal coefficient of viscous forebody drag must still be proven.

This work was done by Stephen A. Whitmore and Timothy R. Moes of **Dryden Flight Research Center.** *Further information is contained in a TSP [see page 1].*

This invention is owned by NASA, and a patent application has been filed. Inquiries concerning nonexclusive or exclusive license for its commercial development should be addressed to the Patent Counsel, Dryden Flight Research Center [see page 1]. Refer to DRC-99-01.

FoilSim: Software for Teaching About Airfoils

Interactive graphical displays help students perform simulated flow experiments.

John H. Glenn Research Center, Cleveland, Ohio

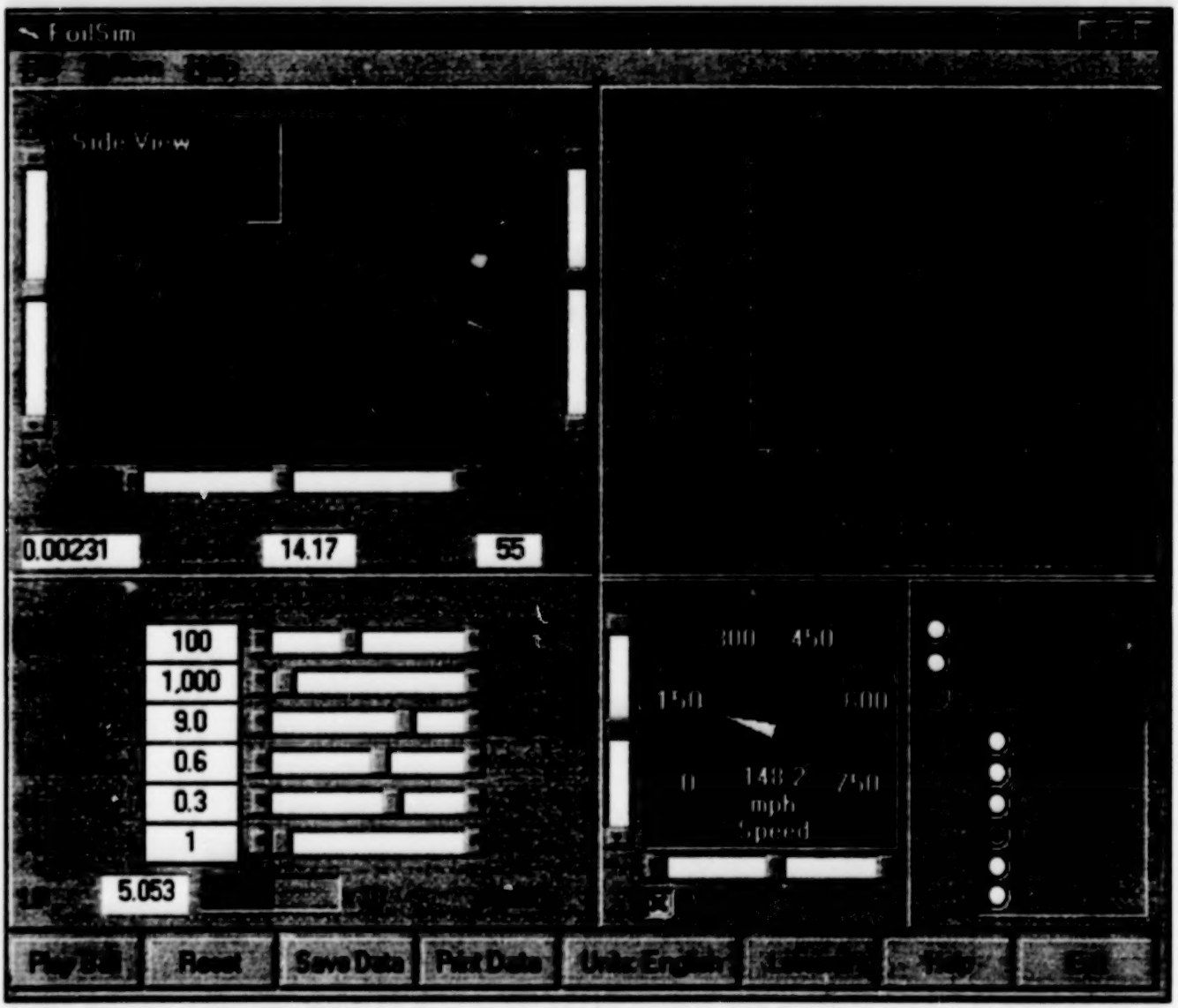

FoilSim Generates an Interactive Display that shows aspects of the flow around an airfoil. Through the controls in the display, the user can explore the effects of design parameters like thickness, curvature, and angle of attack.

FoilSim is a computer program that calculates and graphically depicts information on flows of air around airfoils of various shapes. Although it is useful primarily as a teaching tool to enhance mathematical and scientific curricula, it was derived from "real-life" flow-computing software of engineering quality. To make the underlying flow-computing software useful in education, it was augmented with a graphical user interface that enables students to manipulate the features of the program easily and that guides the students through the learning process. The team that designed FoilSim

combined the highly technical knowledge of scientists with the understanding of experienced educators to generate a product that is not too complex to be understood by students, yet it provides an entertaining and interactive way for students to explore substantial mathematical and scientific concepts.

FoilSim generates an interactive display, called the Airfoil View Panel (see figure), which contains a simulated view of a wing being tested in a wind tunnel with air moving past it from left to right. Students can change the position, orientation and shape of the wing by moving slider controls in the display to vary the parameters of altitude, angle of attack, thickness, and curvature. Other parameters that can be varied are the wing area and the airspeed. The software displays plots of pressure or airspeed above and below the airfoil surface. A simulated probe monitors airspeed and pressure at a particular point on or close to the surface of the airfoil. The software calculates the lift of the airfoil, enabling students to learn factors that influence lift.

Interactive lessons that accompany the program prompt students to engage in problem solving and discovery. These lessons include:

- Factors That Affect Lift
- How Lift Changes
- Flow Field Details
- The Lift Coefficient
- Baseball Lessons

In Baseball Lessons, students learn more about aerodynamics by controlling conditions of a baseball pitch, including altitude (location), speed, and spin.

The overall reaction from FoilSim users has been overwhelmingly positive. A high-school teacher reported that all of his students were using FoilSim and were beginning to "appreciate the process of experimenting." A student obtained a superior rating for a science-fair project that incorporated FoilSim. Parents, flight instructors, and engineers, each having a different reason to use FoilSim, have all expressed their delight with the program.

This work was done by Tom Benson, Bruce Bream, and Beth Lewandowski of **Glenn Research Center**; *John Eglenauer and Ruth Petersen of RMS Information Systems; Roger Storm of Fairview Park City Schools; Darryl Palmer, Jr., of Cleveland State University; and Carol Galica of Thigpen and Associates. For further information, visit the FoilSim web site at http://www.lerc.nasa.gov/Other_Groups/K-12/aerosim/.*

LEW-16711

Apparatus for Attaching Two Spacecraft Under Remote Control

Toroidal bladders are inflated to grasp a rocket nozzle from the inside.

Lyndon B. Johnson Space Center, Houston, Texas

An apparatus called a "pneumatic stinger" has been developed to enable a first spacecraft, operating under remote control, to grasp a second spacecraft that is in orbit or other unpowered flight. The pneumatic stinger, which is mounted on the first spacecraft, is inserted in a rocket-engine nozzle of the second spacecraft, then actuated to grasp the nozzle from the inside, as explained below. Both NASA and the Department of Defense could use this apparatus for servicing satellites. The design of the pneumatic stinger might also be adaptable to soft-docking mechanisms or grappling mechanisms for use on Earth.

The pneumatic stinger offers advantages over an older stinger-type apparatus used to attach a first spacecraft to a rocket nozzle on a second spacecraft. In operation of the older apparatus, an astronaut on the first spacecraft had to position the stinger mechanism in alignment with the nozzle on the second spacecraft, then actuate a trigger mechanism to initiate attachment. In addition, it was necessary for the second spacecraft to be equipped with a structural surface, adjacent to the nozzle, that mated with an interface ring on the stinger and that carried loads. Often, it was not possible to equip a satellite-type spacecraft with a structural surface of this type. In the cases of satellite-type spacecraft that could be equipped with such structural surfaces, the surfaces were required to be of specific shapes and designs. In contrast, the pneumatic stinger is fully automated in that it can be operated without intervention by an astronaut, functions without need for precise initial alignment, and can be used without expensive structural modification of the spacecraft to be grasped.

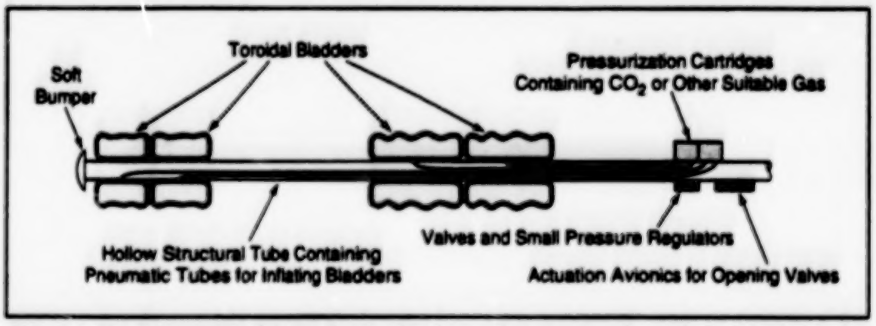

Figure 1. The Pneumatic Stinger Protrudes from a first spacecraft, ready for insertion in the rocket nozzle of a second spacecraft.

Figure 1 shows the pneumatic stinger in its preactivation state. A soft bumper on the insertion end of the stinger prevents damage to the combustion chamber associated with the nozzle. A pair of bladders (two are used for protective redundancy) is located near the insertion end. After insertion of the stinger in the nozzle and combustion chamber, these bladders are inflated into contact with the interior wall of the combustion chamber, thereby capturing the second spacecraft. Two larger bladders are located about midway along the stinger (the exact location depending on the size of the nozzle); these bladders are inflated (see Figure 2) to center the stinger and react loads through the nozzle to the structure that attaches the nozzle to the second spacecraft. The gas for inflation is supplied from redundant pressurization cartridges through valves and regulators controlled by electronic circuits.

The inflated inner and outer bladders trap the throat between them. The axial reaction of the inner (combustion-chamber) bladders is balanced by the opposite reaction of the outer (nozzle) bladders; this balance serves to preload the stinger into controllable contact with the nozzle. The contact between the bladders and the nozzle is soft; it does not damage the nozzle because the bladders hold the nozzle at rel-

atively uniform pressure, which the nozzle is designed to withstand. Moreover, the preload is applied in all directions, so that axial loads and moments can be applied to and through the stinger and nozzle to control the orientation of the second spacecraft.

In addition to the advantages mentioned above, the pneumatic stinger offers two other advantages over the stinger in the older docking apparatus:

- After insertion of the stinger, the only action required is opening of pressurization valves. Consequently, it is easy to fully automate the operation of the pneumatic stinger.
- Use of the pneumatic stinger is relatively inexpensive.

This work was done by William C. Schneider of **Johnson Space Center**. *Further information is contained in a TSP [see page 1].*

This invention has been patented by NASA (U.S. Patent No. 5,735,488). Inquiries concerning nonexclusive or exclusive license for its commercial development should be addressed to the Patent Counsel, Johnson Space Center, (281) 483-0837. Refer to MSC-22745.

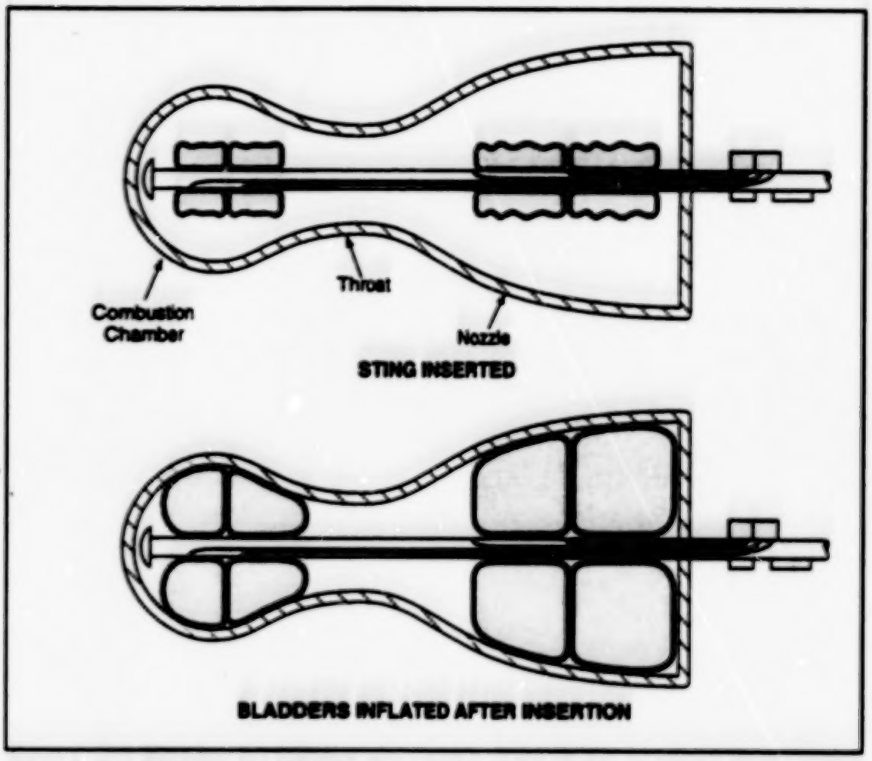

Figure 2. The Bladders Are Inflated after insertion of the stinger, so that the stinger grasps the nozzle and combustion chamber firmly yet gently from the inside.

BLANK PAGE

Machinery

Hardware, Techniques, and Processes

BLANK PAGE

Small Hybrid Rocket Engines Fabricated via X-Ray Lithography

X-ray lithography would extend the lower limit on practical sizes.

NASA's Jet Propulsion Laboratory, Pasadena, California

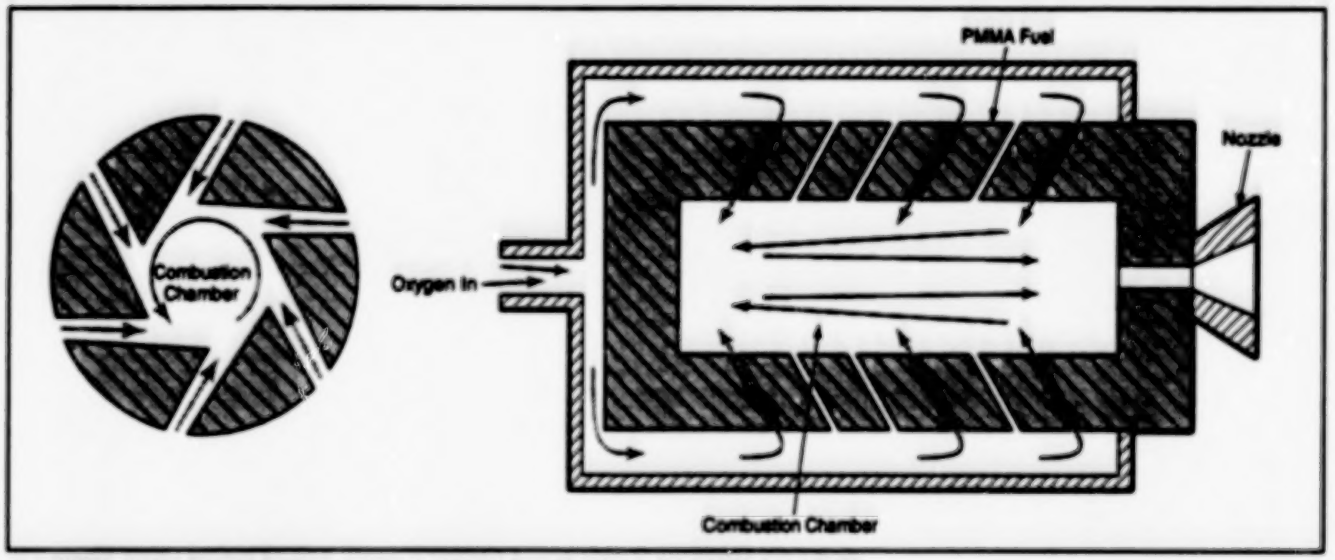

In a PMMA Vortex Rocket Engine, oxygen is injected through holes in the PMMA fuel cylinder.

Small hybrid rocket engines of a proposed type would burn specially shaped hollow cylinders of solid fuel containing slanted oxygen-injection channels, as shown in the figure. These engines would exploit a vortex flow phenomenon associated with the radial inflow of the oxygen in the channels. The fuel/flow-channeler cylinders could be supplied in or as cartridges that could fit into reusable receptacles.

The basic vortex-combustion engine concept, using poly(methyl methacrylate) (PMMA) as the solid fuel, has been investigated previously. The novel aspect of the present proposal pertains to the size range and the means of fabrication. The proposed engines would be too small for conventional machining, making it necessary to fabricate the engines (including the fuel/flow-channeler cylinders) by use of x-ray lithography.

Small engines of the proposed type could be used in their own right as thrusters for small spacecraft or as experimental small-scale prototypes of larger thrusters. After further research to gain better understanding of the vortex flow in question, it might become feasible to apply the vortex-combustion engine concept to develop improved combustion chambers in fossil-fuel power stations, boilers, retorts, gas-fired home furnaces, and turbojet engines.

This work was done by Victor White of Caltech for **NASA's Jet Propulsion Laboratory.** *Further information is contained in a TSP [see page 1].*

NPO-20594

Miniature Turbomolecular Pump for High Vacuum

Pumping speed would be greater than that of a similarly sized ion pump.

NASA's Jet Propulsion Laboratory, Pasadena, California

A proposed miniature turbomolecular pump would be a prototype of high-vacuum sources for a forthcoming generation of miniature, portable mass spectrometers and other scientific instruments. The miniature turbomolecular pump would be an attractive alternative to currently available high-vacuum sources (including most commercial off-the-shelf turbomolecular pumps), which are too bulky and power-hungry to be practical for use in portable instruments.

The smallest currently available high-vacuum pumps are miniature ion pumps that operate at pumping speeds of <1 liter/second. Prior to the conception of the miniature turbomolecular pump, there were plans to use two miniature ion pumps to provide high vacuum to a developmental portable miniature quadrupole mass spectrometer. The miniature turbomolecular pump would be installed in place of the two ion pumps; its overall size would be similar to that of the combination of two ion pumps but with higher pumping speed.

Like other turbomolecular pumps, the miniature turbomolecular pump would contain rows of rotor blades stacked in alternation with rows of stator blades, the spaces between the blades constituting passageways through which gas molecules would be pumped. The stator blades would be mirror images of the rotor blades. The rotor would be connected by a shaft to an off-the-self dc brushless motor, which would drive the rotor at a blade-tip speed as close as possible to the thermal speeds of the gas molecules to be pumped.

The pump design must be synthesized in an iterative procedure that involves consideration of blade angles, number of blades per row, hub diameter, and of gaps among rotor blades, stator blades, the hub, and the inner wall of the pump housing. The maximum pumping speed and compression ratio at smaller number of stages (pump size), predicted for a given combination of design parameters are evaluated with respect to the gas load or throughput. The resulting optimum parameters are then implemented towards the construction of the pump.

As in other vacuum systems, the miniature turbomolecular pump would be con-

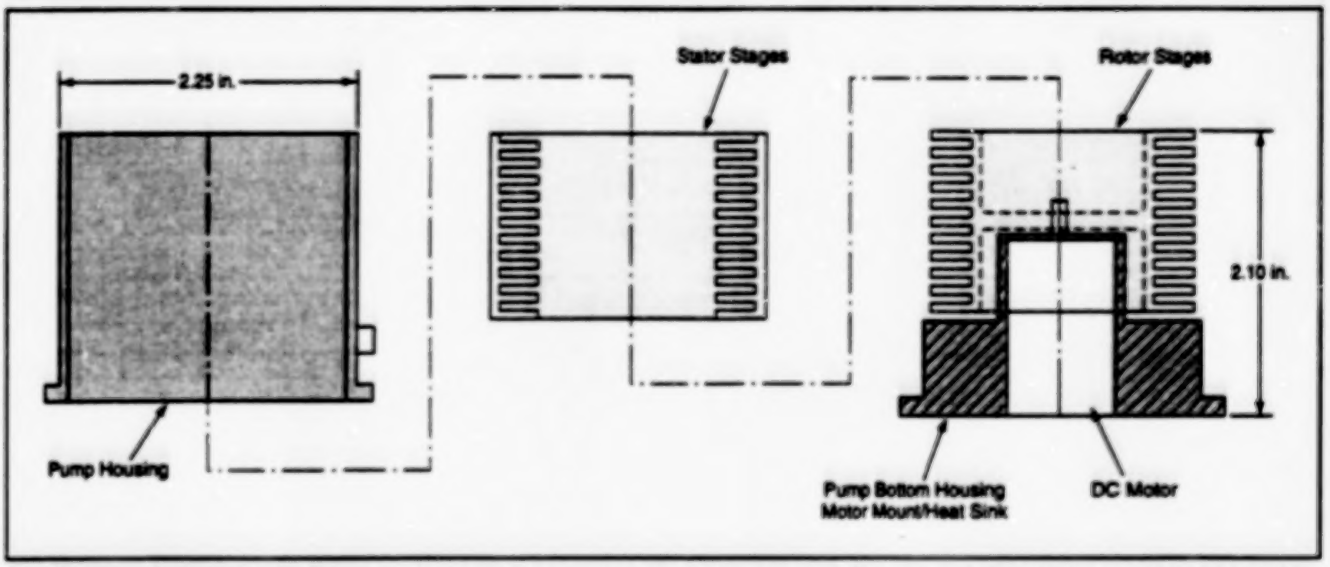

This Miniature Turbomolecular Pump would operate at a pumping rate of 3 liters/second. The rotor and stator blades would be fabricated by electrical-discharge machining.

nected in series with a fore pump that would exhaust to the atmosphere. This will not be necessary for the case of EVA (extra-vehicular-activity) applications and hence a much smaller pump would result. The lowest pressure achievable inside a vacuum chamber depends on the compression ratios of the turbomolecular pump and fore pump.

The figure is a simplified representation of major components of the miniature turbomolecular pump according to the design under consideration at the time of reporting the information for this article. This design is optimized for operation in conjunction with a miniature diaphragm fore pump that provides an inlet pressure of about 1.5 torr (0.2 kPa). The rotor would spin at a speed of 157 krpm. The total compression ratio for air would be 10^5, and the pumping speed would be 6 liters/second. The peak power consumption is estimated at 8 W, decreasing to approximately 0.1 to 0.2 W at maximum rotor speed. Its weight excluding the backing pump is estimated to be about 11 oz (312 g).

This work was done by Vachik Garkanian of Caltech for **NASA's Jet Propulsion Laboratory**. *Further information is contained in a TSP [see page 1].*
NPO-20530

Mathematics and Information Sciences

Hardware, Techniques, and Processes

BLANK PAGE

Robust and Efficient Generation of Cartesian Meshes for CFD

This algorithm is suitable for component-based flow geometries.

Ames Research Center, Moffett Field, California

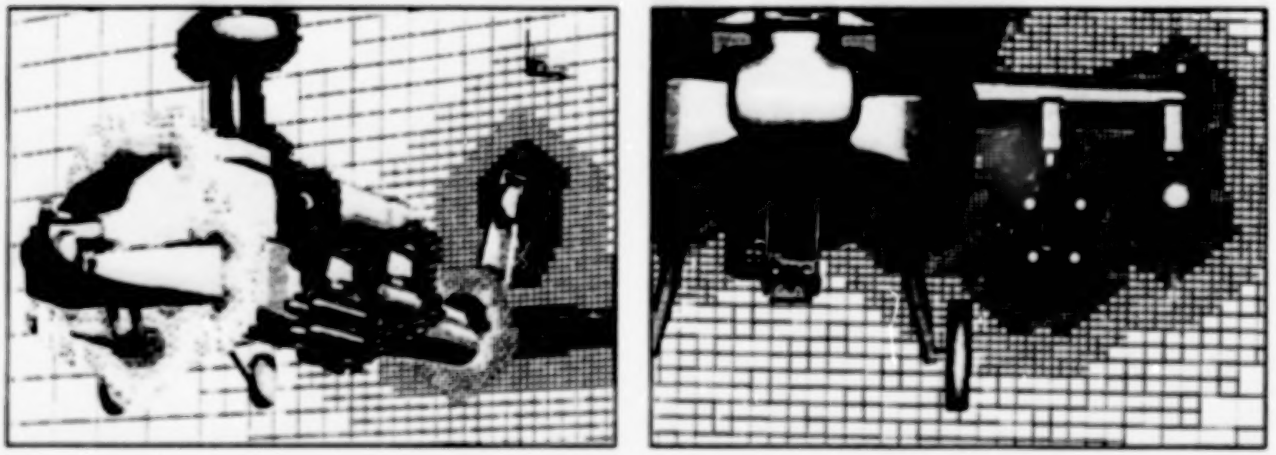

A Cartesian Mesh Around an Attack Helicopter, containing 5.81×10^6 cells, was generated by the algorithm in a computation time of 320 seconds on a moderately powerful engineering computer workstation with a central processing unit running at a speed of 195 MHz.

An algorithm for the robust and efficient generation of Cartesian meshes for computational fluid dynamics (CFD) has been developed. The algorithm generates a mesh for computing the flow in a region bounded by solid components that have prescribed sizes, shapes, positions, and orientations, and that may be moving with respect to each other.

Some background information is prerequisite to a summary of the algorithm. Unlike some other computational grids, Cartesian meshes are not body-fitted. The cells of Cartesian mesh are hexahedral (more specifically, right parallelepipeds) and some cells can extend through surfaces of solid components in the computational domain. Therefore, part of any Cartesian-mesh-generation algorithm must include identification of cells that intersect solid surfaces and the flagging or removal of cells that are completely internal to the solid objects and thus not in the flow field. The remaining cells are then considered general volume mesh elements.

Fundamentally, in Cartesian approaches, one trades the case-specific problem of generating a body-fitted surface mesh for the more general problem of computing and characterizing intersections between hexahedral mesh cells and body surfaces. Thus, all difficulties associated with meshing a given geometry are restricted to a lower-order manifold that constitutes the wetted surface of the geometry.

Unlike the surface cells of a body-fitted mesh, the cells of a Cartesian mesh that intersect the surface are describable without describing the surface itself. In other words, the description of the surface is no longer needed to resolve both the flow and the local geometry. Therefore, efforts to describe the surface can be focused uniquely on the task of resolving the geometry, while computations that involve mesh cells are devoted to a description of the flow. Of course, accurate representations of boundary conditions in cells that intersect surfaces are essential to successful Cartesian schemes. This concludes the background information.

The present algorithm implements a two-phase strategy: In the first phase, intersections among all components are found and used to complete the description of the wetted surface, so that all surface-intersecting Cartesian cells found subsequently are guaranteed to be exposed to the flow field. The remaining mesh-generation problem can then be treated as if it were a single-component problem. In the second phase, the volume mesh is generated.

The component-intersection part of the algorithm is a robust geometry-oriented subalgorithm that, among other things, accommodates the surface triangulations commonly used to describe the surfaces of solid components. This subalgorithm utilizes adaptive precision arithmetic, and it includes a tie-breaking routine that automatically and consistently resolves geometric degeneracies. The worst-case computational complexity of the intersection subalgorithm is of the order of $N \log N$, where N is the number of triangles describing the geometry.

The volume-mesh-generation part of the algorithm takes the intersected surface triangulation as input and generates the mesh through division of hexahedral cells of an initially uniform coarse grid. This approach preserves the ability to refine the mesh to different degrees in different directions, consistently with the local geometry, thereby making it possible to avoid generating excessive numbers of Cartesian cells in three dimensions. The mesh-generation subalgorithm has linear asymptotic computational complexity, with memory requirements that total approximately 14 words per cell. The figure depicts part of a mesh generated by the algorithm.

This work was done by M. J. Aftosmis and J. E. Melton of **Ames Research Center** *and M. J. Berger of the Courant Institute. Further information is contained in a TSP [see page 1].*

This invention is owned by NASA, and a patent application has been filed. Inquiries concerning nonexclusive or exclusive license for its commercial development should be addressed to the Patent Counsel, Ames Research Center [see page 1]. Refer to ARC-14275.

Software for Viewing Results of Computational Simulations

This program aids visualization of data from large-scale parallel processing.

John H. Glenn Research Center, Cleveland, Ohio

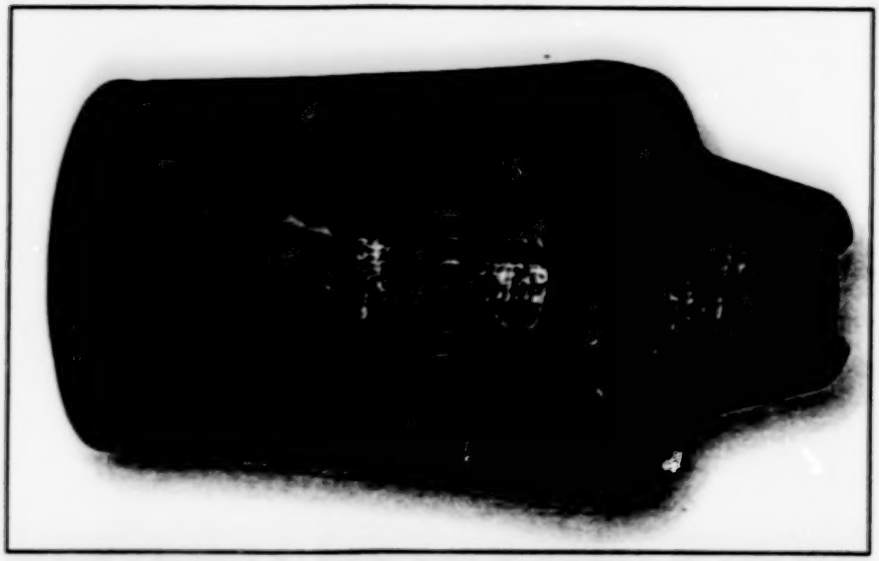

This Image of the Interior of a Turbofan Engine was generated by pV3. Images like this one are used to display results of Navier-Stokes computations of flow in the engine.

Parallel Visual 3 (pV3) is an interactive computer program that provides selected displays of data generated in numerical simulations — especially simulations that involve parallel processing. pV3 was originally designed to aid in the visualization of numerical results from computational fluid dynamics (CFD) calculations on unstructured as well as structured computational meshes, but can also be used to display data from other calculations and to display intermediate computational results for diagnosis of simulation software.

Parallel processing is used to reduce significantly (relative to serial processing) the time needed to perform complex numerical simulations of engines for purposes of design or analysis. Parallel processing is becoming common in industries (aerospace, automotive, financial, and oil-exploration) that rely heavily on computational simulations. As a result, there is a need for new software tools that designers and analysts can use to interact with computational simulations while the computations are in progress. pV3 is an innovative visualization-aiding software tool that satisfies part of that need. pV3 enables the viewing, steering, and understanding of results of a simulation while the results are being generated in a distributed parallel computing environment.

pV3 was developed to support work in the emerging field of parallel application programs, as part of the participation of Glenn Research Center in the High Performance Computing and Communication (HPCC) project. HPCC began to develop large-scale simulations that exceeded the computing capacity of any current single shared-memory computer. The ability of pV3 to make visible all the data generated by distributed computers made it possible for HPCC and derivative projects at Glenn Research Center and in industry to perform simulations that they were unable to perform before.

The figure presents an example of an image of the interior of a turbofan engine that contains 5,000 airfoils, generated by pV3. Optionally, a display containing images like this one could comprise still or moving pictures. Such a display could not be generated by any other currently available software running on any currently available distributed computing hardware.

This work was done by R. Haimes of Massachusetts Institute of Technology and Gregory J. Follen of the Computing and Interdisciplinary Systems Office at **Glenn Research Center**. *Further information is contained in a TSP [see page 1].*
LEW-16712

Program Generates Graphics To Help in Planning Space Flights

Data can be presented as overlays on world maps for quick analysis.

Goddard Space Flight Center, Greenbelt, Maryland

The Mission Planning Graphical Tool (MPGT) computer program provides a mouse-driven graphical representation of data on a spacecraft and its environment, for use in planning a space flight. MPGT is designed to be a generic software tool that can be configured to analyze any specified Earth-orbiting spacecraft mission.

The data are presented as a series of overlays on top of a two- or three-dimensional projection of the Earth. As many as six spacecraft orbital tracks can be drawn at one time. Position data can be obtained by either an analytical process or by use of ephemeris files. If the user chooses to propagate a spacecraft orbit by use of an ephemeris file, then files in Goddard Trajectory Determination System (GTDS) format must be supplied. The MPGT user's guide provides a complete description of the GTDS format so that the user can create the files. Other overlays include ground-station antenna masks, solar and lunar ephemerides, coverage by the Tracking Data and Relay Satellite System (TDRSS), a field-of-view swath, and orbit number. From these graphical representations, an analyst can determine such spacecraft-related constraints as communication coverage, infringement of interference zones, availability of sunlight, and visibility of targets to instruments.

The presentation of time and geographical data as graphical overlays on a world map makes possible quick analyses of trends and of parameters related to time. For instance, MPGT can display the propagation of the positions of the Sun and Moon over time, shadowing of sunrise and sunset terminators to indicate day and night for spacecraft and the Earth, and color coding of spacecraft-

orbit tracks to indicate day and night for spacecraft. In the case of the three-dimensional display, the user specifies a vector that represents a position in the universe from which the Earth is to be viewed. From the "viewpoint," the user can zoom in on, or revolve about, the Earth. The zoom feature is also available with the two-dimensional display.

MPGT also provides alphanumeric data on spacecraft orbit tracks, celestial bodies, and TDRS positions. The user can scroll through the spacecraft and celestial data; that is, can propagate data into the future or past. The program contains data files of world-map continent coordinates, contour information, antenna-mask coordinates, and a sample star catalogue.

Since the overlays are designed to be mission-independent, it is not necessary to modify the software in order to satisfy requirements for various spacecraft. All overlays are generic, with communication-zone contours and spacecraft terminators generated analytically on the basis of spacecraft-altitude data. Interference-zone contours are specified by the user through text-edited data files. Spacecraft-orbit tracks are specified via Keplerian, Cartesian, or Definitive Orbit Determination System (DODS) orbit vectors. Finally, all overlays related to time are based on an epoch supplied by the user.

A user-interface subsystem enables the user to alter any system parameter through a series of pull-down menus and pop-up data-entry panels. The user can specify, load, and save profile data files; control graphical presentation formats; enter a DOS shell; and terminate the operation of the system. MPGT includes a menu option for printing all graphical images by use of any printer compatible with the HALO Professional software. The user-interface subsystem automatically checks for errors in, and validates, all input data from either a file or keyboard entry. A help facility is also provided.

MPGT includes a utility subprogram, called "ShowMPGT," which displays screen images that were generated and saved by previous use of MPGT. Specific sequences of images can be recalled without having to reset profile-related parameters.

MPGT is written in FORTRAN, C, and Macro Assembler for use on IBM-PC-compatible computers running MS-DOS version 3.3 or higher. Necessary hardware includes 620KB of core (random-access) memory; Enhanced Graphics Adapter or Video Graphics Array; 1.5MB of either floppy- or fixed-disk storage capacity; a 1.44MB, 3.5-in. (8.89-cm) floppy-disk drive, and an 8087, 80287, 80387, or compatible processor. The software supports the use of a mouse, which is optional.

This program was written by Lisa Mazzuca, James Jeletic, and Stan Watson of **Goddard Space Flight Center**. *Further information is contained in a TSP [see page 1].*

GSC-13669

END

10-22-99